Design and Development of Rolling and Hopping Ball Robots for Low Gravity Environment

by

Laksh Deepak Raura

A Thesis Presented in Partial Fulfillment
of the Requirements for the Degree
Master of Science

Approved April 2016 by the
Graduate Supervisory Committee:

Jekan Thanga, Co–Chair
Spring Berman, Co-Chair
Hyunglae Lee
Erik Asphaug

ARIZONA STATE UNIVERSITY

May 2016

ABSTRACT

In-situ exploration of planetary bodies such as Mars or the Moon have provided geologists and planetary scientists a detailed understanding of how these bodies formed and evolved. In-situ exploration has aided in the quest for water and life-supporting chemicals. In-situ exploration of Mars carried out by large SUV-sized rovers that travel long distance, carry sophisticated onboard laboratories to perform soil analysis and sample collection. But their large size and mobility method prevents them from accessing or exploring extreme environments, particularly caves, canyons, cliffs and craters.

This work presents sub- 2 kg ball robots that can roll and hop in low gravity environments. These robots are low-cost enabling for one or more to be deployed in the field. These small robots can be deployed from a larger rover or lander and complement their capabilities by performing scouting and identifying potential targets of interest. Their small size and ball shape allow them to tumble freely, preventing them from getting stuck. Hopping enables the robot to overcome obstacles larger than the size of the robot.

The proposed ball-robot design consists of a spherical core with two hemispherical shells with grouser which act as wheels for small movements. These robots have two cameras for stereovision which can be used for localization. Inertial Measurement Unit (IMU) and wheel encoder are used for dead reckoning. Communication is performed using Zigbee radio. This enables communication between a robot and a lander/rover or for inter-robot communication. The robots have been

designed to have a payload with a 300 gram capacity. These may include chemical analysis sensors, spectrometers and other small sensors.

The performance of the robot has been evaluated in a laboratory environment using Low-gravity Offset and Motion Assistance Simulation System (LOMASS). An evaluation was done to understand the effect of grouser height and grouser separation angle on the performance of the robot in different terrains. The experiments show with higher grouser height and optimal separation angle the power requirement increases but an increase in average robot speed and traction is also observed. The robot was observed to perform hops of approximately 20 cm in simulated lunar condition. Based on theoretical calculations, the robot would be able to perform 208 hops with single charge and will operate for 35 minutes. The study will be extended to operate multiple robots in a network to perform exploration. Their small size and cost makes it possible to deploy dozens in a region of interest. Multiple ball robots can cooperatively perform unique in-situ science measurements and analyze a larger surface area than a single robot alone on a planet surface.

To my parents Reeta Raura and Deepak Raura

ACKNOWLEDGEMENTS

Firstly, I want to express gratitude to my Chair and Mentor Dr. Jekan Thanga for his guidance, support and motivation. His constant encouragement helped me explore area which I would not have worked in otherwise. This has helped me grow as an engineer and widen my portfolio of work. I am thankful to Prof. Thanga the amount of effort he puts in for the success of students at SpaceTREx Lab.

I have been fortunate to have Prof. Spring Berman, ASU as my co-chair. She has been very helpful and was available whenever I needed her help. I would like to thank Prof. Erik Asphaug, ASU who has be one of the corner stones of SpaceTREx Lab. I would like also thank Prof. Hyunglae Lee, ASU.

I would like to thank my colleagues and friends at SpaceTREx, Lab. I would like to specially thank Aman Chandra for valuable inputs and ideas and Andrew Warren for help with construction of testbeds for experiments. Lastly, I want to thank all my friends and folks who have been a major part of my journey at ASU and who motivated me throughout my research.

TABLE OF CONTENTS

Page

LIST OF TABLES…….vii

LIST OF FIGURES……ix

CHAPTER

1. INTRODUCTION……..…….....1

Background…….....1

Problem Statement…...……5

Scope……...…….6

Objective……...…...6

2. LITERATURE REVIEW…..……..7

Spherical Robots……..……..…….……7

Hopping Robots……..…….……..10

Gravity Compensation Methods for Space Robot Testing……15

3. METHODOLOGY……..……..21

Design Goal……..…….21

Robot Design…….22

External Shell Design and Drive Train.....28

CHAPTER Page

Hopping Mechanism Design…….…….36

Electronics……..42

Control Software……50

Experimental Setup……51

4. RESULTS AND DISCUSSION……57

Robot Performance in Lunar Gravity……57

Robot Performance in Martian Gravity…….65

Performance of Hopping Mechanism……67

5. CONCLUSION……..68

Conclusion…….68

Future Work……...68

REFERENCES……69

APPENDIX……...72

A DATA COLLECTED BY ROBOT FOR EXPERIMENTS……..72

B MASS PROPERTIES AND POWER BUDGET……. …78

LIST OF TABLES

Table Page

1. List of few experimental and deployed rovers…… ……3
2. Parameters for drive train design……..…..……...30
3. Calculated separation angle for different grouser height……..……...35
4. Comparison between ZigBee, Wi-Fi and Bluetooth……...…….…….....45
5. Specification for LOMASS…...……...……53
6. Data for Multiple Runs on Levelled Sand Surface , 10 mm Grouser Height and Lunar Gravity……59
7. Data for Multiple Runs on 10˚Slope on Sand Surface, 10 mm Grouser Height and Lunar Gravity……...……61
8. Data for Multiple Run on Small Rocky and Gravel Surface, 10 mm Grouser Height and Lunar Gravity……63
9. Data Collected by Robot on Levelled Sand Surface , 10 mm Grouser Height and Lunar Gravity……..…….73
10. Data Collected by Robot for 10˚Slope on Sand Surface, 10 mm Grouser Height and Lunar Gravity……....74
11. Data Collected by Robot for Small Rocky and Gravel Surface, 10 mm Grouser Height and Lunar Gravity……75

Table Page

12. Data Collected by Robot for Levelled Sand Surface , 7 mm Grouser Height and Lunar Gravity……...76

13. Data Collected by Robot for Levelled Sand Surface, 10 mm Grouser Height and Martian Gravity……77

14. Mass Budget of Robot for Design……...79

15. Power Budget for Robot……..80

LIST OF FIGURES

Figure Page

1. Mare Tranquillitatis and Diagram LROC Oblique Image [1]……..…1

2. Lunokhod 1 Rover Developed by Soviet Union [2]...…….2

3. RATLER Robot from Scandia National Laboratory [4]...……..4

4. Spherical Robot Developed by Universite De Sherbrooke [6]...…….7

5. View of Kickbot [7]…….8

6. SMIPS Conceptual Robot Design [8]…….…….9

7. SMIPS Model and Possible Movement Description [8]……..……9

8. Inflatable Robot Developed by NCSU [9]……...…….……10

9. The Microbot System Concept and Major Modules [10]…….…….11

10. The MIT Diamond Dielectric Elastomer Actuator [10]…….…...11

11. 7g Hopping Robot Developed at EPFL [12]……..…12

12. Schematic Diagram of First Generation Mechanism [13]…….13

13. Schematic View of Second Generation Hopper [13]……14

14. Sand Flea Robot Developed by Sandia Laboratory [14]……...14

15. Hopping Robot by Torquer or Reaction Wheel [15]…….15

16. Planar Air-Bearing Microgravity Simulator [18]……..16

17. AERCam Air-Bearing Table Robot [19]……..16

18. Diagram of Cartesian GC System Supporting SM^2 [23]……..17

Figure Page

19. Diagram of the Boom GC System Supporting SM^2 and Payload [23]……..18

20. Micro-g Emulation System [25]……19

21. Active Response Gravity Offload System (ARGOS) Developed by NASA [27]……...20.

22. Mobile Simulator……...20

23. CAD Model of Front View of Ball Robot…….21

24. Exploded View of 1st Iteration of Robot……23

25. Exploded View of 2nd Iteration of Robot……...24

26. CAD Model of Core of Robot ……..25

27. CAD Model of the Upper Section of Robot Core.……...…….25

28. CAD Model of Center Section of Robot Core.…….26

29. CAD Model of Lower Section of Robot Core.…….27

30. Micro Metal Gear Motor with 1000: 1 Gearbox…….……..31

31. Motor with Mounting...…….32

32. Mounting Hub for Wheels……..……...33

33. Diagram to Show Parameters for Wheel Design [16]……...34

34. Wheel with Grouser...……35

35. CAD Model of Hopping Mechanism…….36

36. CAD Model of Hopper Arm.…….37

37. CAD Model of Snail Cam ……37

38. Sequence of Operation of Hopping Mechanism..……..39

Figure Page

39. Steel Flat Spring for Robot…..……...40

40. Geared Motor for Hopping Mechanism……..……..41

41. System Architecture of the Robot.……42

42. Raspberry Pi A+ Board……..43

43. Adafruit DC Motor shield for Raspberry Pi……..43

44. Arduino Nano Board……44

45. ZigBee Module with Breakout Board……45

46. Raspberry Pi Camera...……..46

47. Raspberry Pi Multiplexer Board...…….46

48. Encoder for Micro Gear Motor..……47

49. ACS712 Current Sensor..……..48

50. Li – Ion Battery……..48

51. DC-DC Voltage Regulator……49

52. Power Distribution Diagram of Robot……..49

53. Output File from Data Logger……...50

54. CAD Model of LOMASS system…….51

55. Carriage with Trolley and Suspension Cable……52

56. Strut Channel Mounted on Trolley.……...52

57. Tension cable for preventing twisting…….…..54

58. Robot for Experiment……....54

59. Wheel with 7 mm Grouser……....55

Figure Page

60. Wheel with 10mm Grouser……....56

61. Plot of Robot Speed and Power Vs Time for Levelled Sand Surface, 10 mm Grouser Height and Lunar Gravity…….……...57

62. Plot of Robot Speed Vs Power for Mobility on Levelled Sand Surface, 10 mm Grouser Height and Lunar Gravity…...…….58

63. Plot of Robot Speed and Power Consumption Vs Time for 10˚Slope on Sand Surface, 10 mm Grouser Height and Lunar Gravity..……...…….60

64. Plot of Robot Speed Vs Power for 10˚Slope on Sand Surface, 10 mm Grouser Height and Lunar Gravity…….……...60

65. Plot of Robot Speed and Power Consumption Vs Time for Small Rocky and Gravel Surface,10 mm Grouser Height and Lunar Gravity……..……..61

66. Plot of Robot Speed Vs Power for Small Rocky and Gravel Surface, 10 mm Grouser Height and Lunar Gravity……..…….…….62

67. Plot of Robot Speed and Power Consumption Vs Time for Levelled Sand Surface, 7 mm Grouser Height and Lunar Gravity……..…….....63

68. Plot of Robot Speed Vs Power Consumption for Levelled Sand Surface, 7 mm Grouser Height and Lunar Gravity…….…….…….....64

69. Plot of Robot Speed and Power Consumption on Levelled Sand Surface, 10 mm Grouser Height and Martian Gravity…….65

70. Plot of Robot Speed Vs Power Consumption for Levelled Sand Surface, 10 mm Grouser Height and Martian Gravity……..……...66

Figure Page

71. Test for Operation of Hopping Mechanism at Simulated Martian Gravity……...67

CHAPTER 1

INTRODUCTION

1.1 Background

The formation and evolution of our solar system still has many unanswered questions. This has driven the humankind to explore other planetary bodies to better understand their geology and geohistory. The possibility of human colonization of these planetary bodies, a second safe haven from Earth adds to the drive. Asteroids and meteorites are considered to be the remains of solar system formation. Therefore, studying them is important to answer these questions. Geologists have been studying the terrains and

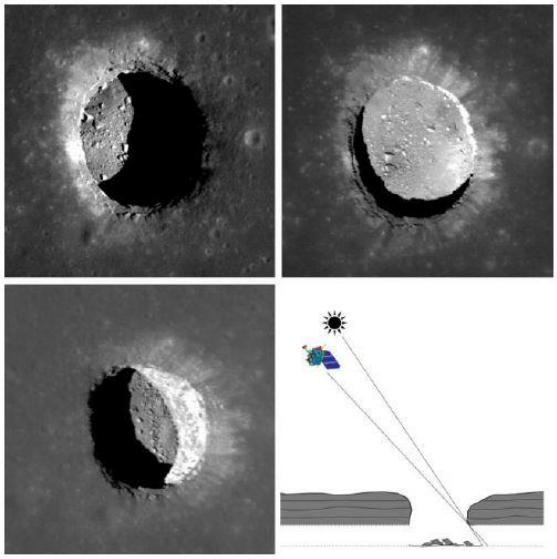

Figure 1 - Mare Tranquillitatis and Diagram LROC Oblique Image [1]

environment on these bodies to find correlation between the formation of earth and other bodies in the solar system. Studying features like ridges, cliffs and pits provide details about the layers of rock formation which are key to understanding the history of formation. Craters are other regions of interest on planetary bodies as they contain

remains of the asteroids and meteorites after impact. The craters themselves based on how much they have weathered provide a record of geohistory. Pits on the Moon could one day host a permanent human base. Evidences from Lunar Reconnaissance Orbiter Camera (LROC) features like Marius Hill and Mare Tranquillitatis have collapsed into a lave tubes with skyline [1] and could be ideal for human a base because they provide shelter from radiation, micro-meteorites and has relatively benign temperature of -25˚c.

Robots have now become one of the primary tools in exploration and study of on other planetary bodies. Earlier exploration were done first by fly by missions to the planetary bodies, followed by orbiting mission then enable long-term remote sensing. Improvement in space technologies and the growing demand from planetary scientists for in-situ science analysis and sample collection has driven the demand for robots to be landed on planetary bodies of interest. The in- situ exploration has allowed the scientist to

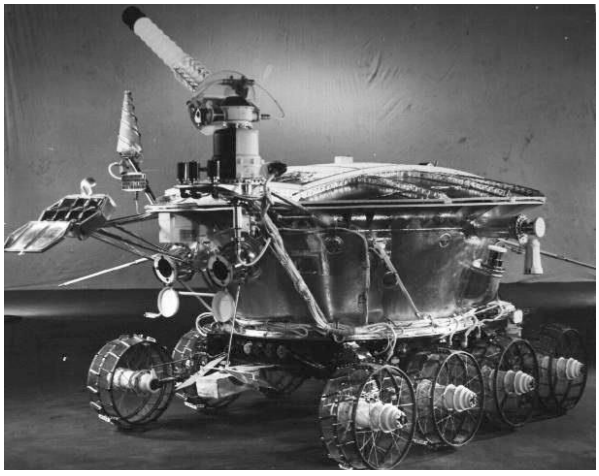

Figure 2 - Lunokhod 1 Rover Developed by Soviet Union [2]

study the formation and evolution of these bodies. Robots have aided the search for essential components of life like water, organic compounds etc. which are precursor to life. This in turn has helped understand the possibilities for human habilitation on them in

future. Multiple missions have explored Moon and Mars, our closest neighbors. There is still a lot to be explored and understood about our neighboring planetary bodies.

In 1970's, two rovers were deployed by Soviet Union on the lunar surface. Though the missions failed to achieve any science goals, this marked the start of an era of use of remote controlled robots for exploration. Since, then, multiple rovers have been deployed on Moon and Mars. NASA has already deployed four rovers on Mars for exploration and to perform in-situ science experiments. These rovers are sophisticated and can perform on board analysis for soil composition and perform sample collection. Their ability to move long distances and collect sample helps to collect data which is more reliable and conclusive.

Rovers	**Developers**	**Properties**
Surveyor Lunar Rover	NASA	50 kg , experimental robot
Marsokhod	Lavochkin/Trans Mash	75 kg, max 30˚slope
Lunokhod	Lavochkin/Trans Mash	756 Kg/840 kg, operated on moon
Lunar Roving vehicle	NASA	620 kg, manned vehicle operated on moon
Spirit rover	NASA	185 kg, operated on mars
Opportunity	NASA	185 kg, operated on mars, still operational
Curiosity (Mars Science Laboratory)	NASA	900 Kg, still in operation

Table 1 – List of Few Experimental and Deployed Rovers [3] [4]

These rovers are generally size of an SUV. The size, weight and sophisticated architecture makes them very costly to build, transfer and deploy them to the site for exploration. Their size and cost prevents them from exploring regions like ridges, cliffs and craters. Each rover is precious enough to risk entrapment. Also it's risky to drive the robot down an uneven slopes. All of these factors severely constrain operation of these

rovers. Low-cost platforms are required to complement these large rovers to perform high risk, high reward science missions.

Micro rovers possess an advantage in this respect. Micro rovers or robots are small mobile robots that can also travel to areas accessible by large rovers. In some instances, these rovers can access extreme terrain inaccessible to large rovers. They have a mass ranging from 1 – 5 kg [5]. These may be self-contained with respect to power, controls

Figure 3 - RATLER Robot from Scandia National Laboratory [4]

and navigation. They can work in regions most rovers can operate in but also explore region not accessible using large rovers. They might not be able to perform sophisticated operations individually but they can operate in groups or in addition to larger rover to enhance the performance. They can be used as scouts or can identify areas of interest for bigger rovers. By working in swarm, they multiply science return in contrast to well-equipped static lander or single rover. Figure 3 shows the RATLER robot developed by Scandia National labs for lunar exploration [4]. It is much easier to land and transport these rover in comparison to larger rover. On planets like Mars where there is atmosphere

these rovers can be deployed using parachutes and aeroshell. Technologies like Capsule System Advanced Development system developed in late 1960's which was designed to land 30-50 kg payload could be used [3] and therefore, reducing the cost of mission.

But the size and mass of the micro rovers pose some challenges with design and operation. One major problem is with size energy available for operation is reduced as battery storage is significantly reduced and very small area is exposed for charging using solar cells. Computer size and memory is also limited due to size, therefore, this limits the ability to perform on board processing of data. Solution could be to process data via ground station on earth. Only essential data processing for navigation and control can be performed on board. Direct communication with earth via the DSN is complex and energy intensive. Alternative is to use nearby space assets. Therefore, an orbiter can be used relay data to earth or the robot can to be coupled with larger rover for communication. The other issue to overcome obstacles larger than the size of the robot. Due to mass the tractive force is very low for wheeled robots. Multiple wheels also poses issue with maneuverability of the robot.

1.2 Problem Statement

Mobility is one major issues with micro rovers. Scientists and researchers have proposed various mobility methods like wheels, legs etc. Wheels have been the most reliable method of mobility for rovers. All the rovers deployed are wheeled. Hopping is another mode of mobility which is very promising. Researchers have tried different methods to perform hopping. Hopping can be advantageous in overcoming obstacles bigger than the size of the micro rovers.

The regions of our interest are ridges and pits which generally have downward slope. Robots that allow for rolling could save lot of energy. The spherical shape is ideal for this. Spherical shape also aids to overcome obstacles and traverse on any surface.

1.3 Scope

The scope of this thesis includes following

1. Design of a spherical shaped robot able to perform mobility on different terrains, gravity and surfaces in laboratory conditions.
2. Design and evaluation of hopping mechanism for the robot in different simulated gravity condition.
3. Testing of robot operation and mobility under simulated Lunar and Mars gravity conditions.

1.4 Objective

The main objective the thesis is to develop a ball shaped robot with hopping and rolling capabilities for low gravity exploration. The work will include demonstration of a working prototype and evaluation of the robot performance in a laboratory environment.

CHAPTER 2

LITERATURE REVIEW

2.1 Spherical Robots

Multiple spherical shape robots have been developed in past. The spherical shape provides ability for free rolling and ease to overcome obstacles as compared to other rover designs. Spherical robots achieve rolling by either moving external spherical shell or having external two wheels for rolling. This section discuss about different design of spherical robots proposed for space as well terrestrial application.

2.1.1 RoBall

A research group from Universite De Sherbrooke presented spherical robot for low gravity exploration. They proposed a robot encapsulated inside a spherical shell and

Figure 4 - Spherical Robot Developed by Universite De Sherbrooke [6]

it rotates the shell to move. The robot contained internal plateau and all components are mounted on this plateau [6]. Plateau was connected to the external spherical shell on both

side and used one or two motors to move the shell. The robot was controlled using feedback from the inclinometer. The motor speed was controlled based on inclination to maintain center of gravity close to ground. Their first prototype was developed as an entertainment toy but was never tested for performance in planetary condition.

2.1.2 Kickbot

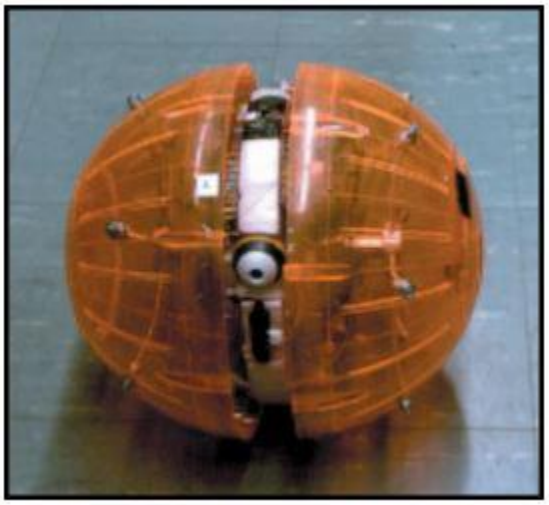

Figure 5 – View of Kickbot [7]

Kickbot [7] was autonomous robot developed by Massachusetts Institute of Technology to roll around and invite people for kick. These robots were had two external hemispherical shell connected to a central section containing drive. The robot had counter weight in the center section which was moved by the motor in front of contact area and the robot fell forward. Since, each hemisphere had dedicated motor and thus, perform differential drive. The robot had very high maneuverability. The robot were designed for terrestrial application.

2.1.3 Inflatable Spherical Robot

Multiple concepts for inflatable spherical robots have been proposed by research

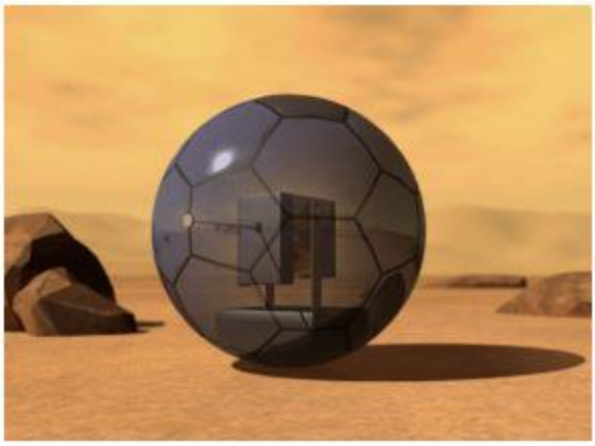

Figure 6 - SMIPS Conceptual Robot Design [8]

team from Uppsala University, North Carolina State University (NCSU) [9] and

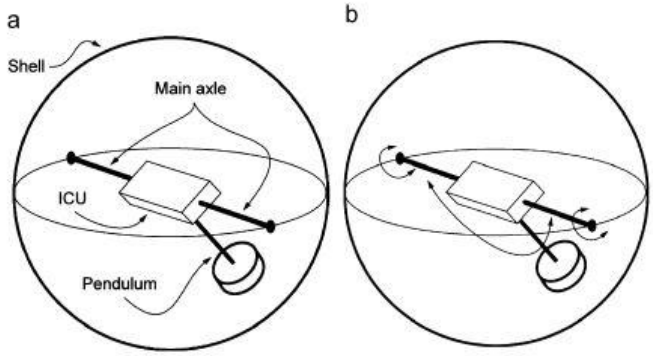

Figure 7 - SMIPS Model and Possible Movement Description [8]

University of Toronto. Research team from Uppsala University proposed a design called Spherical Mobile Investigator for Planetary Surface (SMIPS). The robot has 11 layered, solar cells embedded inflatable spherical shell with a central main axle. The axle has a control unit mounted on the axle and a pendulum is suspended from the axle. The robot rolls by raising the pendulum perpendicular to main axle or by tilting it along the axle. Figure 6 shows the design of the SMIPS and figure 7 shows the method of mobility for

SMIPS. The proposed design was 0.3m in diameter when inflated. The design proposed to be more energy conserving on relatively moderate slopes of upto 30˚. But it would experience difficulties on very rocky environment. A 40 cm spherical robot was estimated to overcome 17 cm high obstacle with initial speed of 2 m/s. It was also

Figure 8 - Inflatable Robot Developed by NCSU [9]

estimated that a 60 cm diameter robot with 8 h of operation would weigh around 10 -15 kg on earth.

2.2 Hopping robots

Hopping poses as a solution for overcoming obstacles larger than the size of the robot. Multiple design for hopping mechanism has been proposed in the past for planetary exploration as well as terrestrial application. This section presents some of the hopping robots and their hopping mechanisms.

2.2.1 Hopping Microbots using Dielectric Elastomer Actuators (DEA)

A micro robot system for planetary exploration was proposed. The robot used

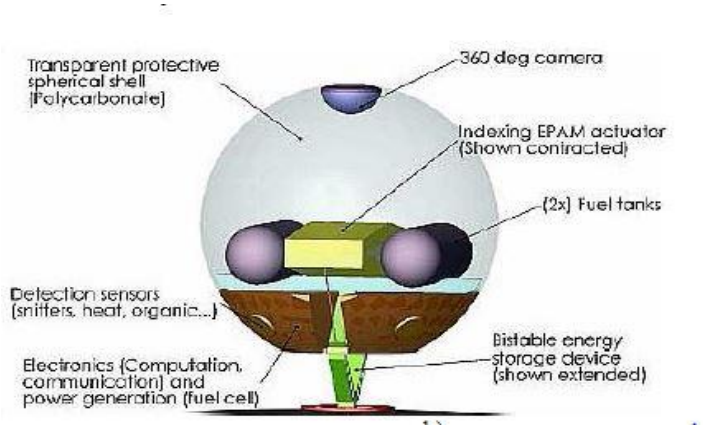

Figure 9 - The Microbot System Concept and Major Modules [10]

hopping, bouncing and rolling for exploration of features of interest like caves and canyon. The robot used Dielectric Elastomers Actuators (DEA) for the hopping. Figure 8 shows the design of the robot and figure 9 shows the hopping mechanism proposed for the microbot. DEA requires very high energy to actuate and also has very slow actuation speed. Therefore, a bi-stable mechanism was developed for hopping and high energy

Figure 10 - The MIT Diamond Dielectric Elastomer Actuator [10]

power sources were required to charge the mechanism over time. The total mass of robot was 100 grams and robot was proposed to power by high energy fuel cells. The mechanism could expand 2.8 times its actual length and produce hope of 10 cm in earth condition. The robot also did not have dedicated mechanism for rolling.

2.2.2 Spring based hopping mechanisms

Most of the robots utilize spring to store energy for hopping. Heritage of spring based systems in space, easy availability and ability to be used repeatedly are few of the driving reason for use of springs. The “Grillo” robot developed at Sant’Anna University

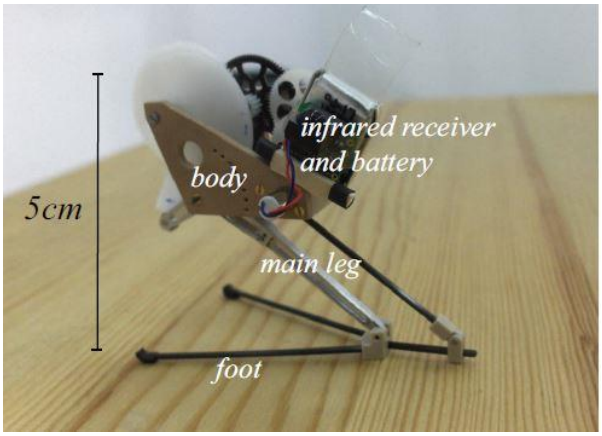

Figure 11 - 7g Hopping Robot Developed at EPFL [12]

[11] and 7g robot developed at EPFL [12] used springs to store energy from rotary motor. These robots used a snail cam to charge the springs. 7g jumping robot can jump 27 times its own size [12]. The mechanism provides good jumping height but provide very little control on the direction of hop.

Burdick and Fiorini proposed design for minimalist jumping robots [13] for

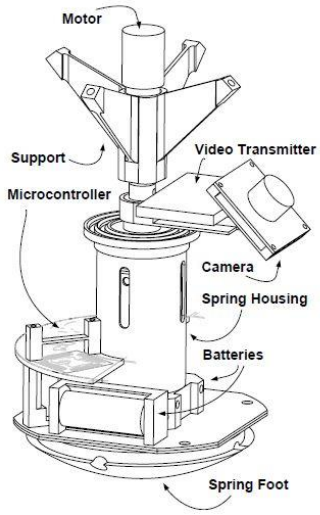

Figure 12 - Schematic Diagram of First Generation Mechanism [13]

planetary exploration. The robot is controlled by a single hopping actuator which uses an over running clutch for mechanism compression and release. An approximately 800 gram robot was able to hop 80 cm high and produce a leap of 30 -60 cm with this mechanism. But mechanism had an efficiency of 20% in converting stored spring energy into hop.. The maximum energy was lost in wasted motion of mass system [13]. In subsequent designs, these issues were resolved and 2nd generation provided better results. One issue was size of the mechanism. The second generation mechanism would fit in 15x15x15 cm^3 space [13] when compressed. Figure 12 shows generation 1 mechanism and figure 13 shows generation 2 mechanism.

Figure 14 - Schematic View of Second Generation Hopper [13]

2.2.3 Other Hopping Mechanisms

Some robots use reaction wheel for hopping. These kind of hopping mechanisms are ideal for exploration of Asteroids. The mechanism works by spinning the reaction

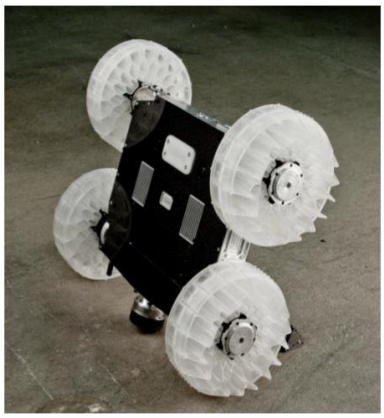

Figure 13 - Sand Flea Robot Developed by Sandia Laboratory [14]

wheel at high speed and then imparting energy to hop by stopping reaction wheel. Sandia laboratory proposed robot called “Sand Flea”. The robot used CO_2 cylinder for charging a pneumatic hopper. The robots were able to hop 50 times the hopper length. But the robot

poses issue for operation in space environment especially in planets with no atmosphere and perform 25 hops in single charge.

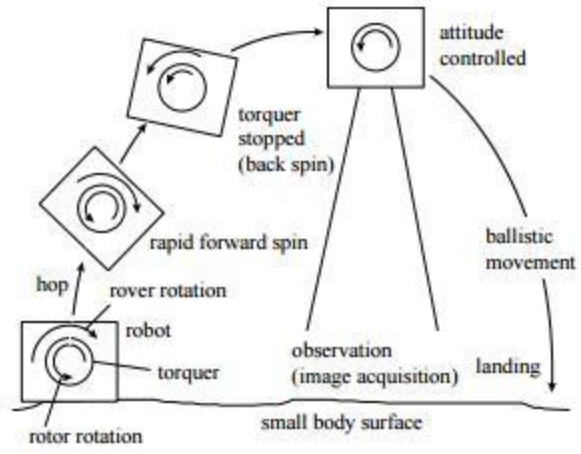

Figure 15 - Hopping Robot by Torquer or Reaction Wheel [15]

2.3 Gravity Compensation Methods for Space Robots Testing

The performance of space robot would vary on target planetary bodies. This is due to different gravity and environmental condition. Gravity has great effect on mobility of robots. Lower gravity would result in lower traction and speeds during mobility. Robots are likely to display more dynamic behavior at lower gravity. Thus, design of robots and their wheels or mobility methods needs to be tested for performance at lower gravity conditions. Therefore, a gravity compensation systems are required to perform realistic testing of such robots on earth.

Different methods have been used to simulate low gravity or provide gravity compensation. In early years of space robotics, low gravity was simulated by using parabolic flights or performing drop tower tests. But duration of these tests is generally few seconds and gravity value is not controllable. This led to development of different systems for gravity compensation or offset systems. One of method is use of air tables. Air table testing is limited to zero gravity and 2-D experiments. Figure 16 and 17 shows examples of the air table system used for space application. The second method widely

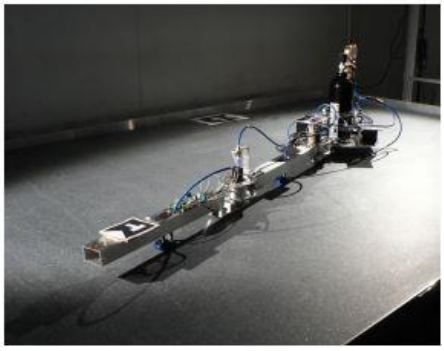

Figure 16 - Planar Air-Bearing Microgravity Simulator [18]

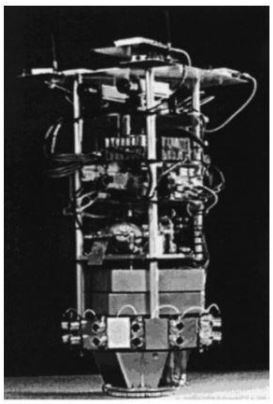

Figure 17 - AERCam Air-Bearing Table Robot [19]

used is neutral buoyancy testing under water. By ballasting the test robot to point buoyancy forces exactly offsets required weight [20], low or micro gravity can be simulated. This system provides 3D simulation as well as long duration tests can be performed. There are several drawbacks to this method though. Water inertia and viscous properties can affect the dynamics of robot [21], thus, collected data may vary from actual operational results. Other drawback are that hardware design has to be water resistant, corrosion resistant and also the sensors for water would be different from that used in space. Above methods also don't allow to simulate performance of mobile robots

on different terrains that robot may encounter on other planetary bodies. One method of gravity compensation for low mass system is suspending using helium balloons [22]. But as the mass for robot increases, balloon size also increases. This induces air drag which may affect results of the test.

Suspending robots using gantry or other support structures like robotic arms is another method widely used for simulation low or micro gravity. Robots are supported from top using cables, harnesses and counterweights mounted on gantry. In some cases, suspension cable support a robotic arm which in turn supports the robot during mobility. This system has advantages over previous methods as by controlling counterweights and

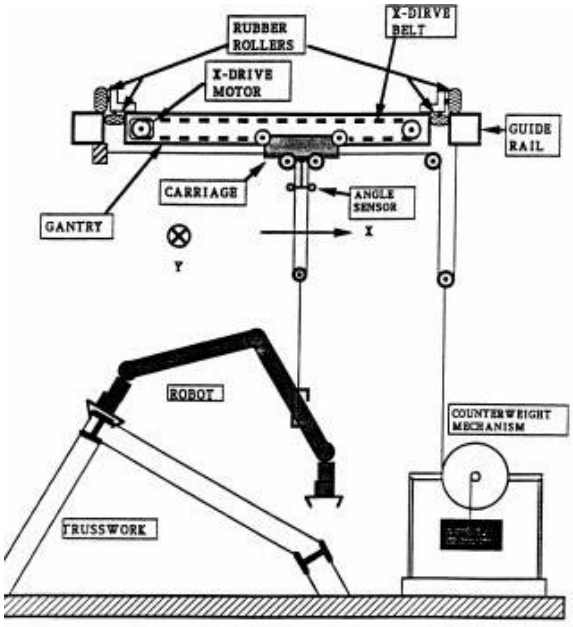

Figure 18 - Diagram of Cartesian GC System Supporting SM^2 [21]

cable tension one can control gravity offset value. Also mobility on different terrains can be tested in 3D. Additional degree of freedom in robot motion can be added by using

gimbals in suspension system. This system of gravity compensation is ideal for mobile robot testing.

Multiple designs for suspension system have been proposed and implemented in past. A group from Carnegie Mellon University, developed two systems for testing their "Self-Mobile Space Manipulator" (SM^2) [21] or space robotic arm. They developed an X-Y-Z gantry system and a boom (cylindrical) system [21]. Figure 18 shows the layout of gantry system. The system includes a passive, vertical counterweight system connected via multiple pulleys to provide constant upward force to offset robot weight. A cantilever carriage provides suspension points for robot. The carriage runs on a guide rail that runs along the Y- axis. Whereas in case of boom design, it also uses identical carriage and rail system as gantry system [23]. Figure 19 shows the layout of boom

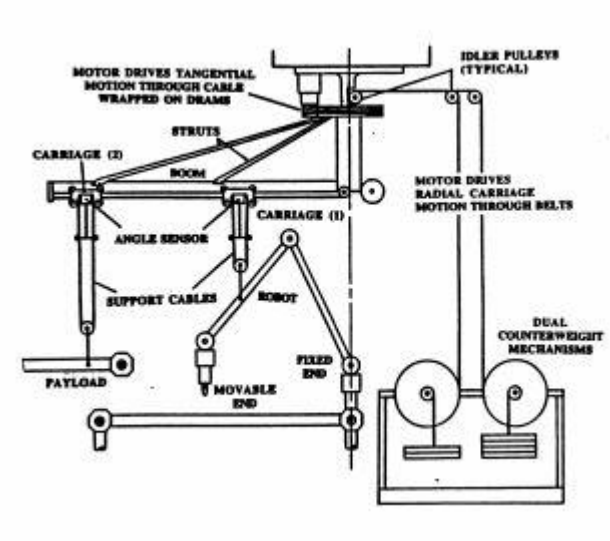

Figure 19 - Diagram of the Boom GC System Supporting SM^2 and Payload [21]

system. This system move in cylindrical coordinate system and is faster than Cartesian system but limited in range. It provides two points for suspension for robots. There are

two counter weight to support two separate loads. Multiple point suspension caused restricted degree of freedom. The system was not couple with an arena for testing mobile robots on different terrain. Similar system was develop at Tokyo Metropolitan Institute of Technology to simulate micro gravity [25]. It used suspension cable to suspend space manipulators or robotic arms and test its operation in low gravity. It has gimbal which enable more degree of freedom. Figure 20 shows layout of system.

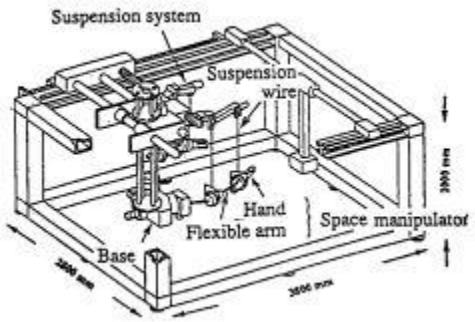

Figure 20 - Micro-g Emulation System
[24]

Many other suspension systems for low gravity simulation have been developed. NASA has developed Active Response Gravity Offload System (ARGOS) for simulating low gravity condition for humans and robots. Figure 21 shows image of the ARGOS. Mobile simulators were proposed for simulating low gravity on outdoor terrains for better results [25]. Figure 22 shows a mobile simulator with rover

Figure 22- Active Response Gravity Offload System Developed by NASA [26]

Figure 21 - Mobile Simulator [25]

CHAPTER 3

METHODOLOGY

3.1 Design Goals

The primary goal for the design of ball shaped robot is developing spherical shape, small size and light weight robot with multiple mobility systems. The mobility systems must be robust and contain simple components to improve the reliability of the system. Spherical shape of robot facilitates free rolling downhill reducing power consumption. Spherical shape also provides more enclosed volume for instrumentation as oppose to other shapes. For a two wheeled design, the center of gravity should be below the center of the robot. This provides the stability to robot and allows for maximum mobility.

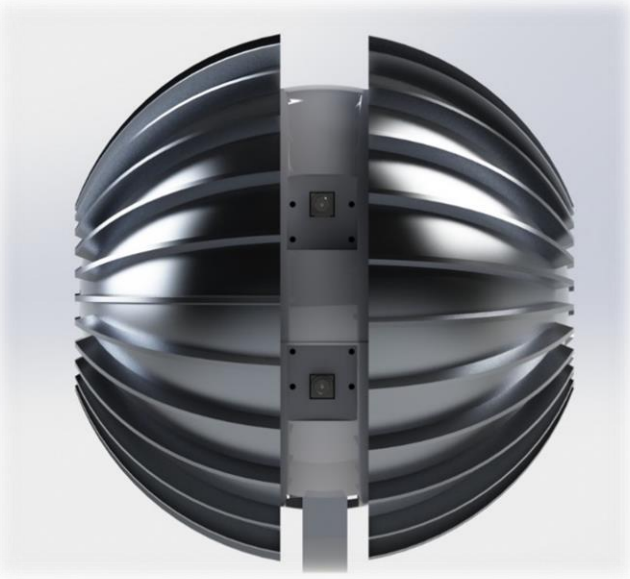

Figure 23- Front View of Ball Robot

One of the primary requirement for design was making robots configurable. As per mission requirements the robot subsystem are bound to change. Therefore, it must be easy to swap out entire subsystems.

3.2 Early Design Evolution and Robot Design

With the specification for the robot defined, the design should be able to accommodate all the electronics, actuators and batteries required for operation. This also helps in maintaining a nominal temperature for the instruments to work as the external temperature can vary over a huge range. For Mars, temperatures vary from -153℃ to 20℃ and for Moon, temperatures are in range of -233℃ to 123℃. Shells provides thermal insulation from these harsh conditions. The scope of this thesis doesn't include thermal analysis of the robot and thus selection of material for it. For the purpose of testing of robot performance, prototypes where build with ABS (Acrylonitrile Butadiene Styrene) plastic using 3D printing technique.

Initial version of robot was designed as a proof of concepts for demonstrating mobility of robot using rolling on smooth marble surface. The robot had three sections divided vertically as shown in figure 24. The left and right hemisphere of the robot contained the robot geared motors and control boards for the robot and the center section contained two batteries mounted in such a way that the center of mass of robot would be close to the geometric center of the robot. There were two separating disk designed to separate the sections and also provided area for mounting batteries and control board. As seen in figure 24 the motor were mounted on the two hemisphere such that they are aligned and

operate as a single rigid body to translate torque from core to the wheels of the robot. As seen in figure 25, robot had two hemispherical wheels on either side of the core. Due to

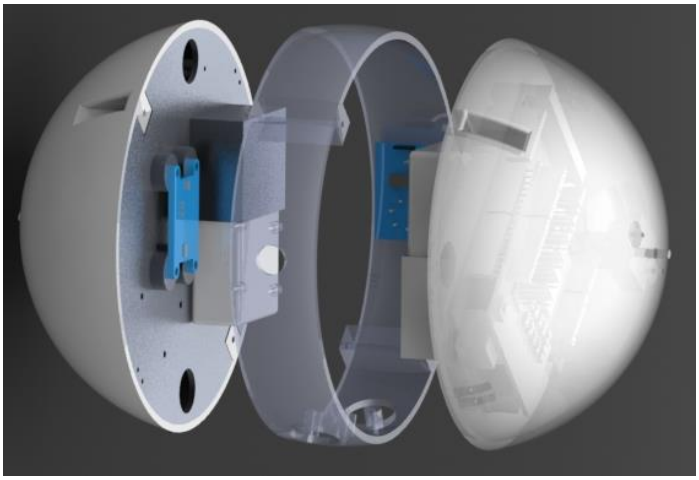

Figure 24 - Exploded view of 1st Iteration of Robot

balance center of mass, the robot was not able to move without contact point between the core of the robot and the ground. This would cause problem in free rolling or tumbling of robot which was one of the reason for spherical shape of robot and thus modifications were required to achieve rolling without contact between ground and robot core. It was found that by shifting the center of mass closer to ground, mobility could be achieved without the requirement for contact of core with the ground.

Hence, for second design only one battery was used as shown in figure 25 and it was mounted such that the center of gravity would be closer to ground. The other sections where not changed. Also, center section was designed with a dead weight to bring the center of mass even more closer to the ground. It was observed that there was excessive slip in wheel due to hard plastic surface. Therefore, a layer of rubber was sprayed on the

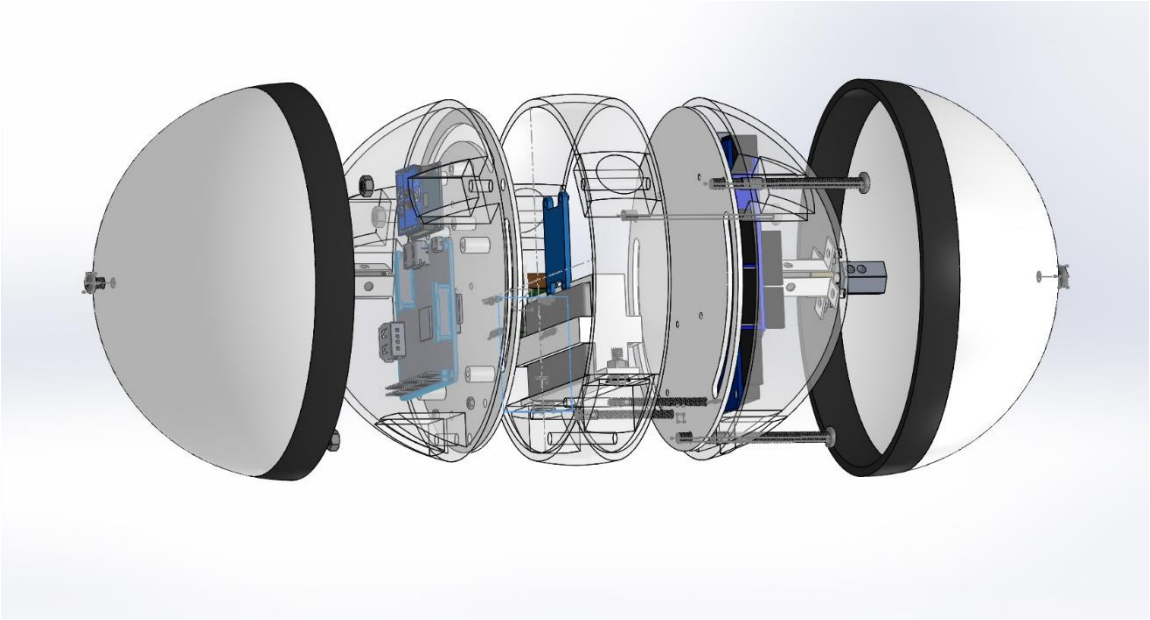

Figure 25 - Exploded View of 2nd Iteration of Robot

wheels to reduce the slip. The robot was able to move on hard marble surface in the laboratory conditions without the contact between the core and the ground. But due to limited space available in the center section major design modifications were required to house secondary mobility system and sensors. Also addition space was required to house the stereo camera pair. Hence, new design was developed with this consideration

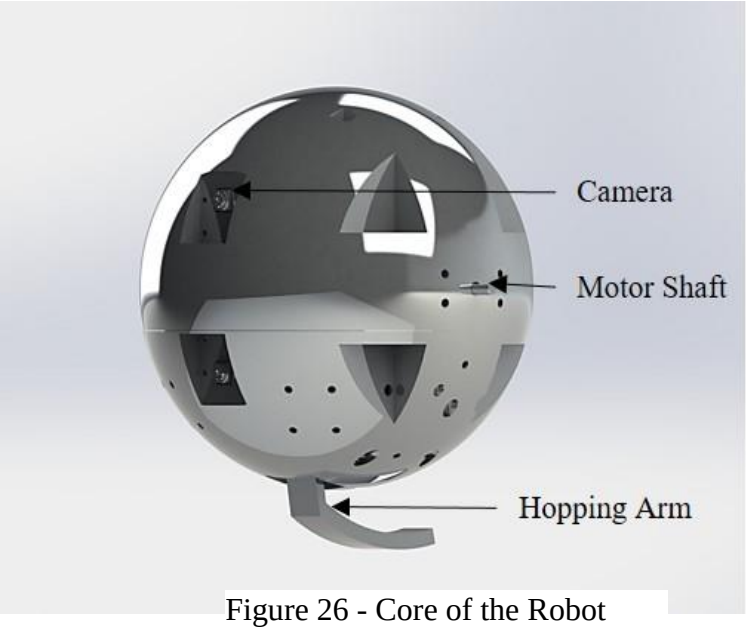

Figure 26 - Core of the Robot

The robot has 150 mm diameter spherical shell that forms the core of the robot. The walls are chosen to be 3 mm thick for mechanical strength. The core is divided into

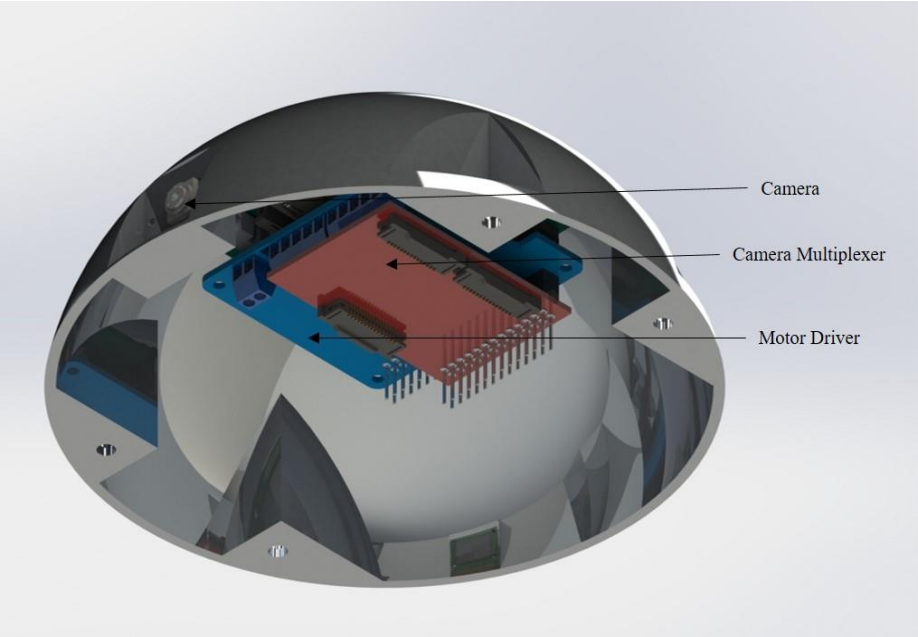

Figure 27 - Upper Section of the Robot Core

three sections with 30 mm wide center section. It was also important that the core has properly bifurcated subsection to meet requirement of adaptability. The subsections were based on functionality for the subsystem and there correlation. There are three sections – Control and Data Handling section, Primary actuation and Power Regulation section and Secondary Actuation and Power Source section. As seen in figure 26 there are four slots in upper and bottom section for holding the sections together using long bolts and nuts.

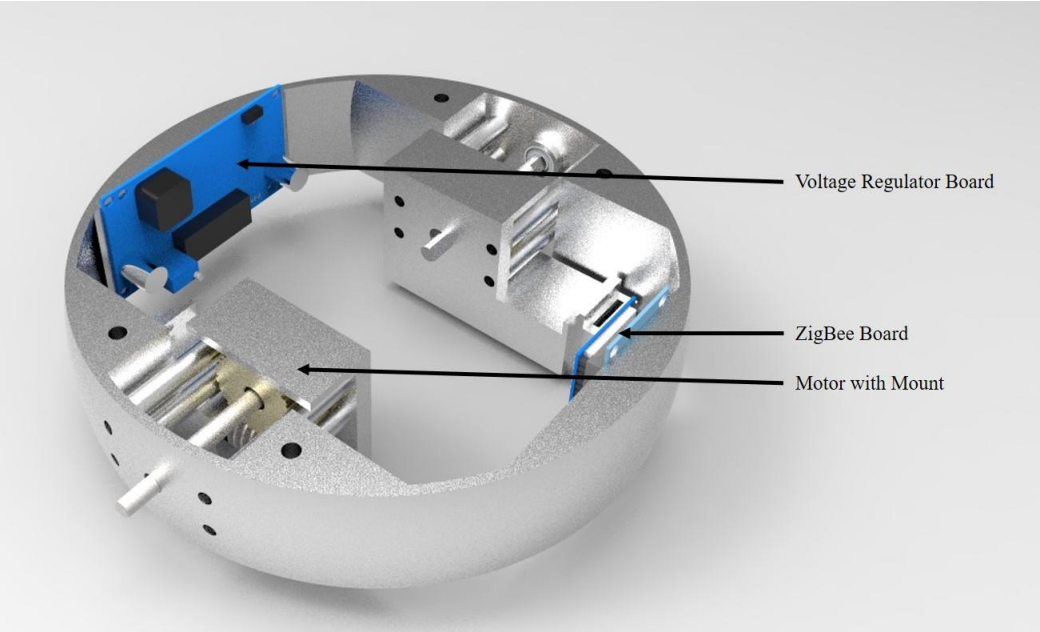

Figure 28- Center Section of the Robot Core

Inner wall of core is used to mount the electronics, actuators and batteries. The top section houses components for command and data handling. The center section has primary actuation system i.e. motors for rolling and power regulator. The bottom section houses components for secondary actuation system i.e. hopping mechanism and battery. The sections are so arranged to provide low center of mass which is primary requirement for mobility of two wheeled robots.

The top section houses the main computer, driver shields for motors and communication boards for robot. The driver shield is mounted on the computer board. Both are screwed to the wall of the robot using screws. A camera interface board is mounted on the shield

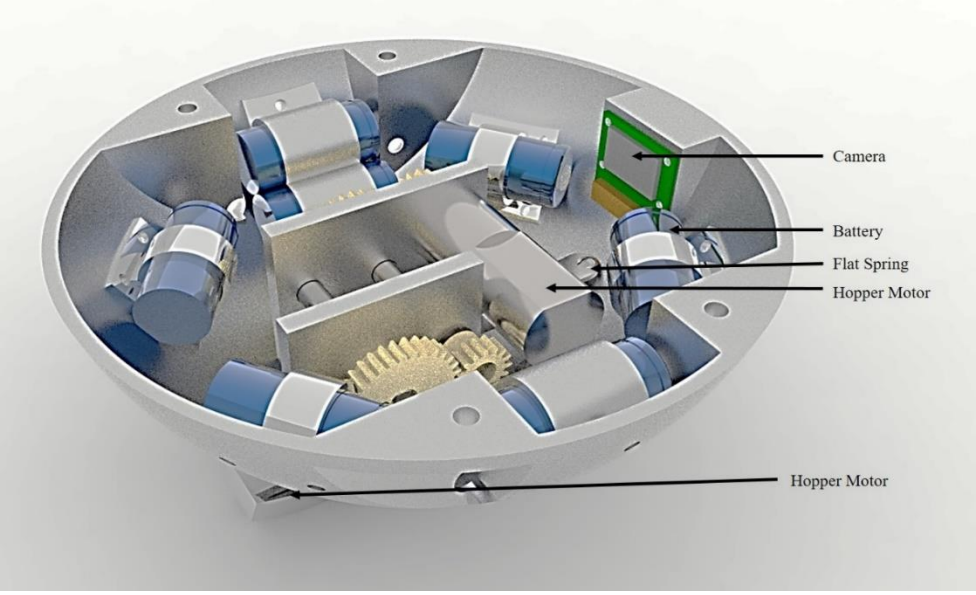

Figure 29- Bottom Section of the Robot Core

and is held in position by mounting headers. There is a mounting slot for the camera modules. A ZigBee communication board is mounted beside the computer. An on/off switch is connected on the opposite side of the camera mount. Motors for rolling are mounted in the center section using a custom mount. Two flat inner surfaces are created by extruding chord section. A DC – DC step down voltage regulator for powering computer and sensors is mounted on the flat section. The bearings are embedded in the wall of center section to support the motor shaft. The bottom section has two 5 mm thick walls in the center of the section for mounting gears and motor for the hopping mechanism. A slot is cut at the bottom of the section for hopper arm. Similar to top section, this section also has a mount for camera module. Eight batteries are mounted to the wall as show in the figure 29 using custom mounts. Flat springs are screwed to the

wall of the bottom section just below the camera mount. These springs store the energy for hopping.

The robot has two external hemispherical shells of 200 mm diameter which encapsulates the robot core. These shells have grouser and act as wheels for the robot. Shells are connected to the robot at their center using an off-the-shelf aluminum hub. The shells mounts on hub using four screws.

3.3 External Shell Design and Drive Train

The drive train is system to transfer torque from motors to the wheels to the robot wheels for rolling. A design with maximum efficiency and low weight is required. The torque must be enough to overcome small obstacles, slopes and travel over sandy terrain. Also the speed reduction should be enough to achieve traction for travel on any terrain.

The wheel diameter and weight of robot are critical for calculating the required torque for traverse on different terrains and obstacles. The traction can be further increased by adding grousers and coating. The wheel are designed to be 197 mm with grouser. The dimension was chosen to encapsulate the core of the robot and the arm of the hopping mechanism. There are two wheels, therefore, the entire mass of the robot is distributed on them. The torque calculation are done based on lunar condition as all test will be done using LOMASS to simulate lunar condition.

The total tractive force required by for mobility of the robot can be defined by

$$F_{TT} = F_{fr} + F_s + F_a \qquad (1)$$

where F_{TT} is the total tractive force, F_{fr} is the total force required to overcome friction, F_s is the total force required to climb slope and F_a is the force required to accelerate. F_{fr} is given by

$$F_{fr} = M_r * \mu_{rr} \quad (2)$$

where M_r is the mass of the robot and μ_{rr} is the coefficient of friction for the surface. Now, F_s is defined as

$$F_s = M_r * \sin\theta_s \quad (3)$$

where θ_s is the slope of the terrain. F_a is defined as

$$F_a = M_r * V_{max}/g * T_a \quad (4)$$

where V_{max} is the maximum velocity of the robot, g is the acceleration due to gravity and T_a is the time to acceleration to maximum speed. Now, based on the tractive load the required motor torque can be calculated by

$$\tau_r = F_{TT} * {}^{D_w}/_2 * \eta \quad (5)$$

where τ_r is the required torque for the mobility of the robot, D_w is the wheel diameter and η is the resistance factor which accounts for additional friction due to grousers on wheels and free counter rotation of robot core. η was taken to be 20% for the robot .Evaluation was done for operating at earth gravity.

Important factor that influence the selection of motor are maximum velocity of robot and maximum slope to be climbed. These factors are limited by the maximum traction force available on a terrain. The traction force can be calculated using

$$F_{T_{max}} = W_n * \mu * D_w \qquad (6)$$

g	Constant of gravity	9.81	m/s^2
μ	Friction Coefficient (sand)	0.6	
μ_{rr}	Rolling Friction Coefficient (Sand)	0.15	
M_r	weight of robot	1.272	kg
θ_s	max grade to be climbed	14	deg
V_{max}	Maximum linear velocity	0.03	m/s
t_a	Time to acceleration	1	sec
R_w	Wheel radius	9.9	cm
W_n	Normal force	0.5	kg
Rf	Resistance Factor (Due to grousers)	20	%
n	no. of wheels	2	

Table 2 - Parameters for Drive Train Design

Where F_{Tmax} is the maximum tractive torque before slipping occurs in each wheel, W_n is the normal load on each wheel and μ is the coefficient of friction between robot wheel

surface and terrain. If the τ_r exceeds summation of F_{Tmax} for all the drive wheel than slipping will occur.

Based on literature, the slip-sinkage relationship for a rigid wheel and soft terrain is

$$z \leq \frac{1}{4} D_w i \qquad (7)$$

Where z is the wheel sinkage and i is the wheel slip. So, with increase in slip the sinkage increases. A permissible value of 20% was set for the slip for design of wheels and motor selection.

3.3.1 Motor Selection

The major criteria for selection of were size of motor, maximum speed and output torque. Equation (5) gives the maximum output torque required for mobility at maximum

Figure 30 - Micro Metal Gear Motor with 1000:1 Gearbox

speed and slope. A micro metal gear motor with 1000:1 reduction was chosen. The motor outputs 9 kg.cm torque with the maximum output speed of 32 rpm at 6V. The motor has an extended shaft for mounting encoder. Motor is 10 x 12 x 29.5 mm in

dimension. The motor delivers enough torque at 6V for the application. But the output speed at 6V high enough to cause enough slippage and thus, lead to sinkage. We would be using PWM (Pulse Width Modulation) to control motor speed of motor. At very low PWM value, the motor power reduces significantly and thus, the torque. So, without additional reduction gearbox enough torque cannot be produced to travel at low speed. The motor needs an additional reduction of 10:1 to achieve desirable speed with enough torque.

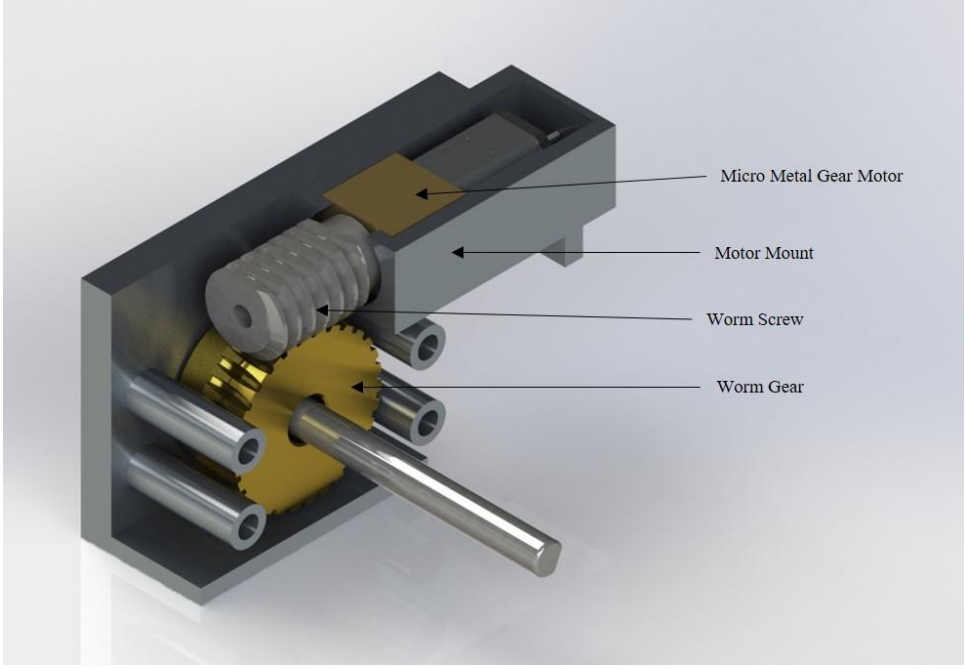

Figure 31 - Motor with Mounting

Now major issues with addition gearbox is space and mounting. With spur gear single stage reduction of 10:1 was not feasible because of size of the driven gear. Other option was to use a worm gear and worm screw set for the reduction. A standard worm

gear set with 3mm pitch worm screw and 30 teeth worm gear where used. As shown in figure 6, a custom mount was designed for mounting the motor and worm gear set. The mount has four mountings holes that attach to center section of the robot. Motor is held in mount by chamber with tolerance fit. The worm screw is connected to the shaft of the motor. Worm gear is mounted below the worm screw on 5mm diameter and 50 mm long shaft as shown in figure 31. The output maximum linear speed of robot after reduction is 200 cm/min at 6V. The resultant torque at 6V is 85.2 kg.cm which is higher than required torque.

Wheels are mounted on the shaft using aluminum hub as shown in the figure 32.

Figure 32- Mounting Hub for Wheels

The hub is mounted on shaft using a set screw. It has 4 M3 size threaded holes for mounting the wheel. This hub was bought off the shelf from Pololu Robotics and Electronics.

3.3.2 Wheel design

Most of the planetary rover wheels are designed with grousers or lugs. This improves the traction of robots in loose soil and also assists in overcoming small

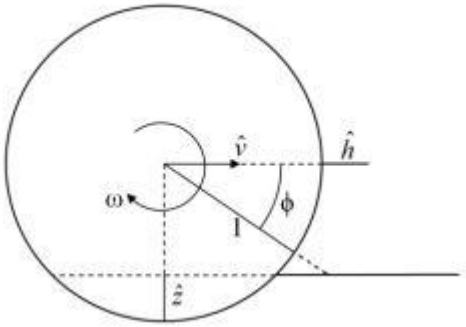

Figure 33 - Diagram to Show the Parameters for Wheel Design [16]

obstacles. The wheel are 197 mm in diameter with 10mm grousers. The wheel are hemispherical in shape and sized to encapsulate the robot core. There are 24 2mm wide grouser that run along the surface of the wheel. There are 4 holes at the center of the wheel as in figure 8 and used to connect the wheels to the output shaft.

The number grouser are decided based on the relation from [16]. The equation (8) give the relation for optimal spacing between grousers such that grouser comes in contact before wheel comes in contact with the ground.

$$\varphi < \frac{1}{1-i}\left(\sqrt{\left(1+\hat{h}\right)^2-(1-\hat{z})^2}-\sqrt{1-(1-\hat{z})^2}\right) \qquad (8)$$

where φ is the angle between the two grouser, i is the wheel slip, $\hat{h}$ is normalized height of grouser i.e. (h/r_w) and $\hat{z}$ is normalized wheel sinkage i.e. (z/r_w). r_w is the radius of the

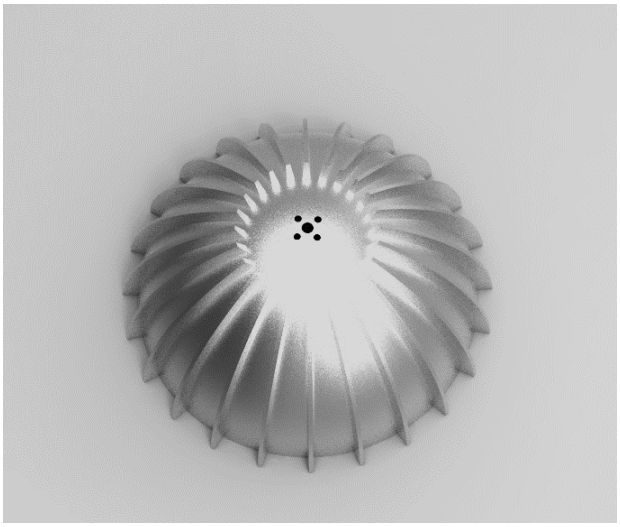

Figure 34 - Wheel with Grousers

wheels. Table 3 shows the calculated value of maximum separation for optimal performance.

Grouser Height	$\hat{h}$	$\hat{z}$	φ
10 mm	0.107	0.1	15.12˚
7 mm	0.074	0.08	9.39˚

Table 3- Calculated Separation Angle for Different Grouser Height

It is considered that only the grousers sink in the terrain maximum height of grouser were taken as sinkage. Based on the calculated maximum angle, wheels were designed with 24 grousers of 10mm height separated by 15˚.

3.4 Hopping Mechanism Design

A secondary mobility system was designed for the ball robot with idea to overcome obstacles larger than the size of robot. Hopping enables the robot to overcome an obstacle twice it size. Also hopping can be used for leaping and thus travelling longer

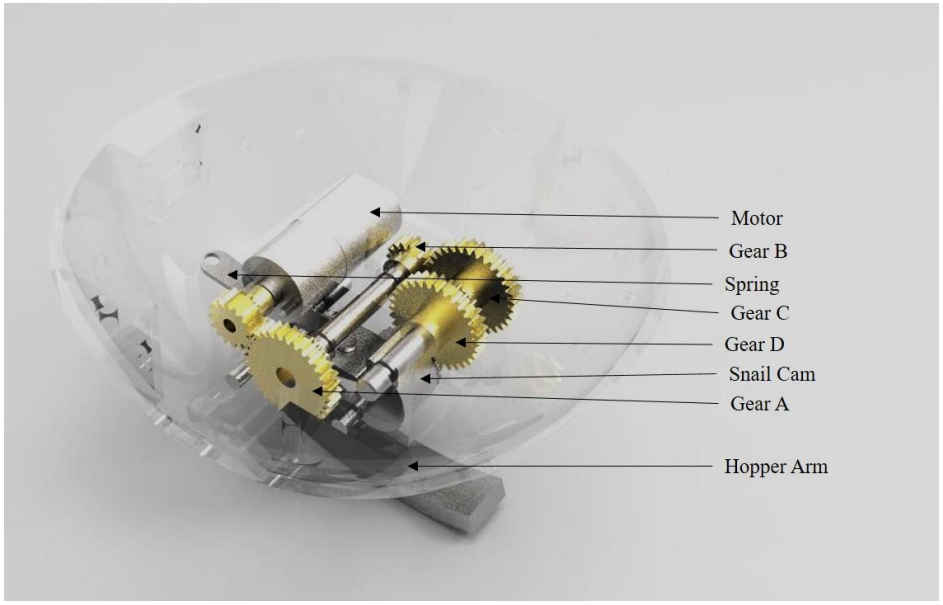

Figure 36 - Design of Hopping Mechanism

distances much quickly as compared to rolling. Major challenge was to develop a

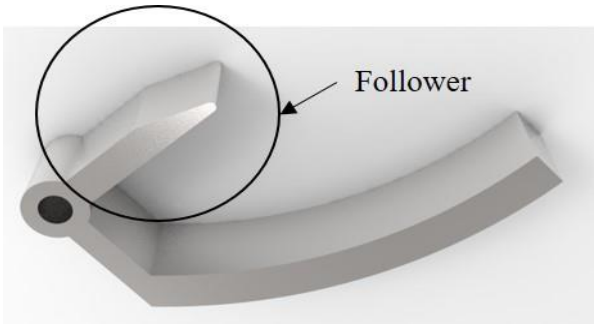

Figure 35 - CAD Model of Hopper Arm

compact robust system that could be packed inside the robot. For hopping two major

requirements are storage of energy for hopping and method to instantaneously release to perform a hop.

Figure 35 shows the design of the hopping mechanism. Mechanism is run by a geared DC motor. A snail cam was designed for charging and instantaneous release of hopper arm which leads to a hop. Figure 36 shows the hopper arm and figure 37 shows the cam designed. Snail cams as shown in figure 37 have a gradually increasing diameter from center to the maximum displacement point. The designed cam has a minimum dimension of 8 mm at the center and 25 mm at the maximum displacement point. The cam is 10 mm wide. This allow for distribution of impact load at hopping on the shaft to be distributed over larger area thus preventing failure of shaft supporting the cam. The hopper arm has two parts the follower which moves over the cam and the curved arm with comes in contact with ground to produce hop. The hopper arm is curved to maintain

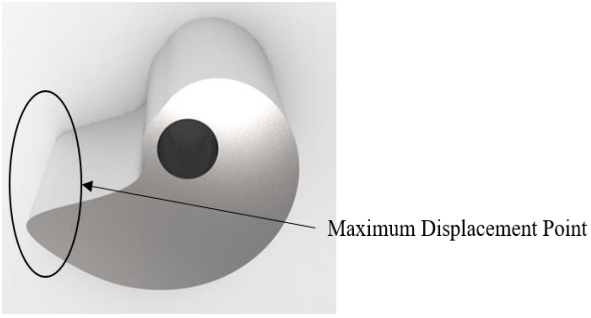

Figure 37 - CAD Model of Snail Cam

the symmetry with shape of robot core. The cam is made of steel because of impact loading in each cycle of hop. Hopper arm is made of aluminum and has a cross section of 5 mm x 10 mm across except at the end of the follower.

The 16 teeth, 32 pitch pinion gear is mounted on the motor. Pinion gear drives a 32 teeth gear A. Another 16 teeth gear B is mounted on the same shaft as gear A. Gear B drives a 32 teeth gear C. Now, 32 teeth gear D is mounted on same shaft as gear C. Gear D drives a 26 teeth gear mounted on same shaft as the cam. When the cam rotates clockwise it gradually charges the arm till follower reaches maximum displacement point. When cam rotates beyond this point, it releases the hopper arm. This allows the robot to hop. Multiple flat springs are used to store the energy before the hop. As shown in figure 35, springs are mounted such that the follower is under spring load. Figure 38 shows the sequence of operation of the hopping mechanism.

A maximum hopping height of 50 cm was chosen for design of hopper mechanism and selection of components. To achieve maximum height of 50 cm, the energy required is given by

$$E_{max} = M_r g H_{max} \qquad (9)$$

Where E_{max} is the potential energy of then robot at maximum height, H_{max}. In ideal case, potential energy at maximum height must be equal to the energy stored in the spring for hopping. Therefore,

$$E_{max} = M_r g H_{max} = {}^{1}/_{2}\, k\theta^2 \qquad (10)$$

Where k is the spring constant and θ is the maximum angular displacement of the spring. The maximum θ for the mechanism is 25.15˚. Based on this, calculated spring constant is

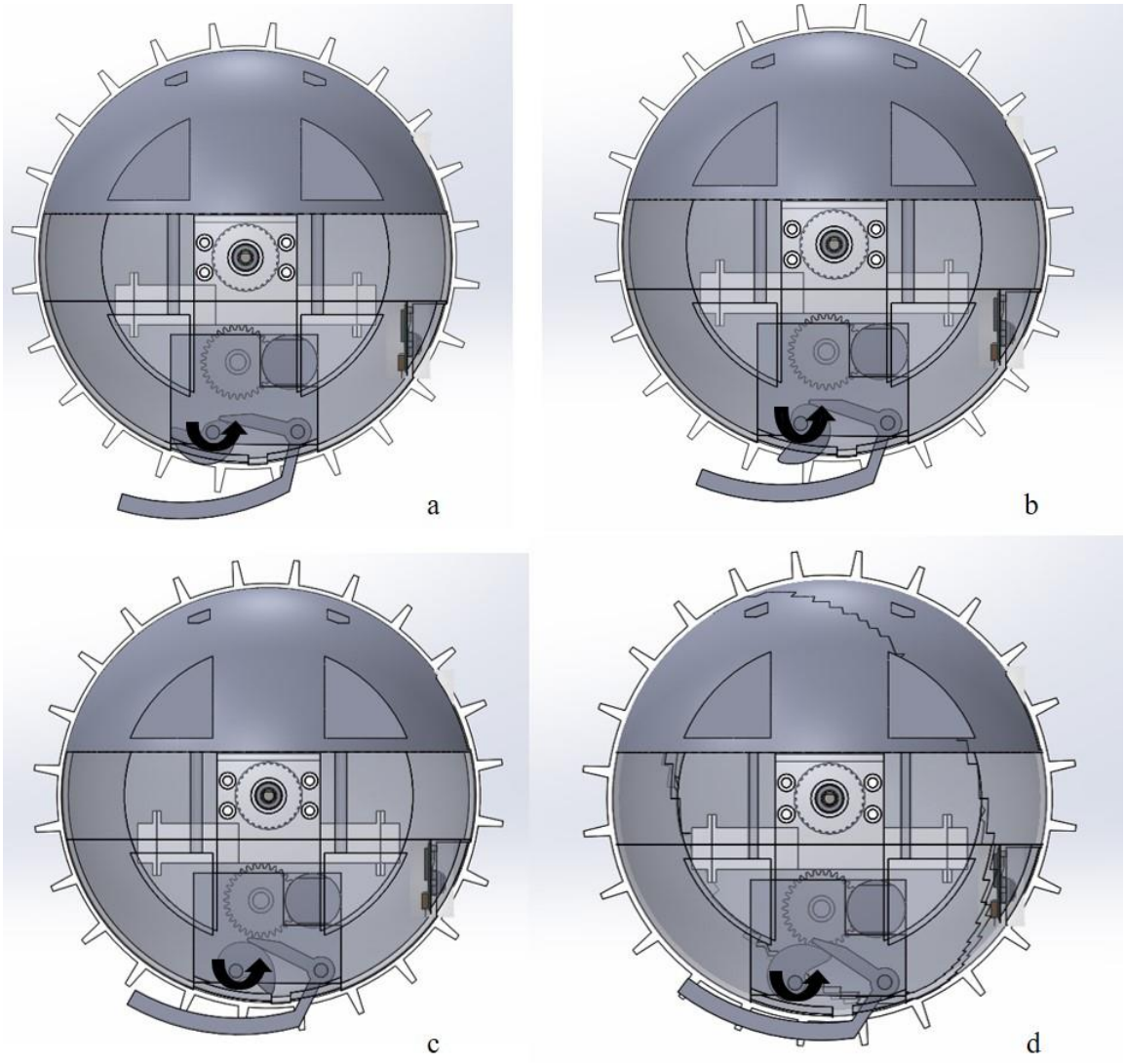

Figure 38 - Operation of Hopping Mechanism

71.308. Flat spring were chosen because of the size constrains. Now, the counter torque to applied by the spring should be

Figure 39- Steel Flat Spring for Robot

$$\tau_s = k\theta \qquad (11)$$

Where τ_s is the torque to be applied by the spring. Based on this the maximum force can be calculated at maximum end of the flat spring.

$$F_s = {}^{\tau_s}/_{L} \qquad (12)$$

Now, the number of flat springs can be calculated using

$$n = \Psi \, {}^{FL^3}/_{Esbt^3} \qquad (13)$$

Where,

$$\Psi = {}^{3}/_{(2+\frac{\acute{n}}{n})} \qquad (14)$$

Where E is the Young's modulus of spring, L is length of spring, s is maximum deflection b is maximum width of spring and t is the thickness of spring. n´ is no of spring of equal length. We have taken all the spring of equal length. From calculation, 6 springs would be required. Figure 39 shows the design of the spring used in the robot.

3.4.1 Motor Selection for Hopping

A geared DC motor was selected for the hopping mechanism. Figure 40 shows the selected motor. The motor output 1.8 kg.cm torque and 90 rpm at 6V. The gear train in

Figure 40 - Geared Motor for Hopping Mechanism

hopping mechanism provides further reduction of 3.25:1. The total output torque at the cam is 5.265 kg cm considering efficiency of gearing to be 90%.

3.5 Electronics

In addition to mechanical design of the robot, electronics are needed to control the robot, acquire data and regulate operations of mechanical system. This section describe the electronic components required for development. Raspberry pi was used as

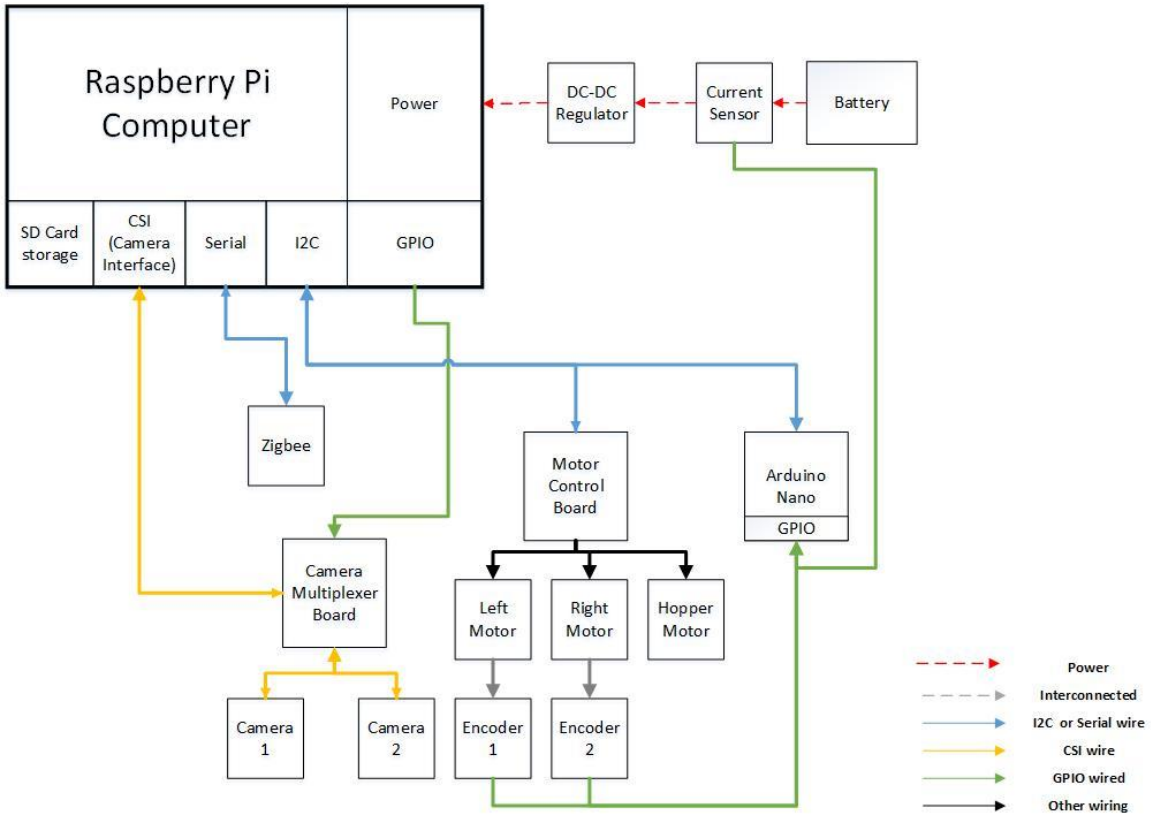

Figure 41 - System Architecture of the Robot

the main computer for data acquisition and communication with the computer for commands. The electronics are powered using eight 3.2V, 650 mAh Li Ion battery connected to provide 7.2V, 2600 mAh.

3.5.1 Control System

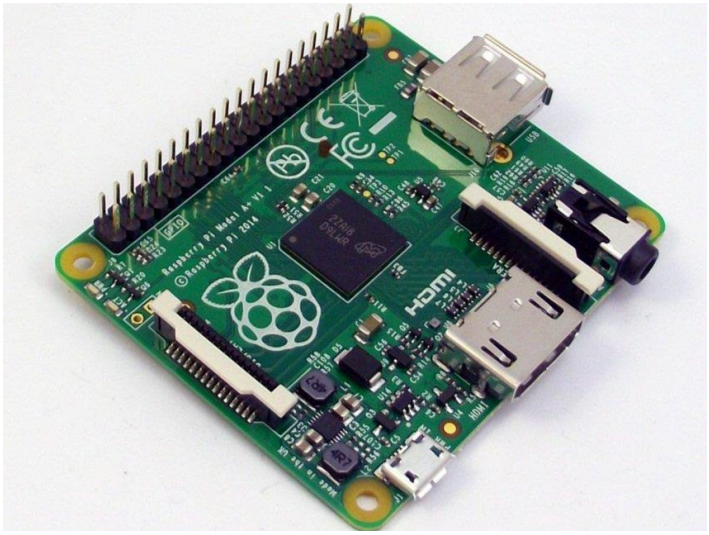

Figure 42 - Raspberry Pi A+ Board

A raspberry pi board was used for sensor data acquisition, image acquisition, communication and command handling. Raspberry Pi A+ board was used because of the

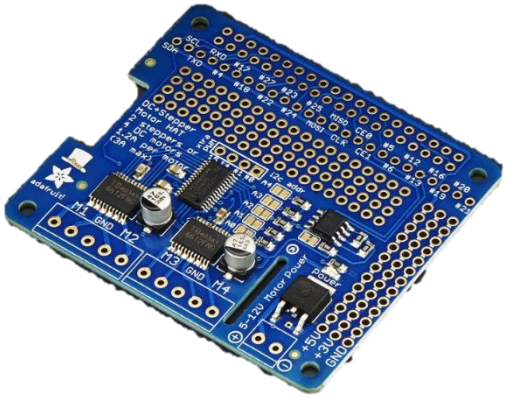

Figure 43 - Adafruit DC Motor Shield for Raspberry Pi

small size factor and easy to integrate camera system. Raspberry pi runs Linux on board which allows easy transition to other boards with Linux in future. Raspberry pi also provides a possibility for multi-tasking using threading.

The Raspberry Pi one serial port, one i2c port and one SPI port, therefore, any type of board or sensor operating at 3.7V can be connected to the raspberry pi. Raspberry

Figure 44 - Arduino Nano Board

pi cannot control motor directly therefore, we need a driver board. We used Adafruit DC motor shield for raspberry pi. The board mounts on the raspberry pi and provides control for four DC motors. The shield communicates with raspberry pi over i2c. Raspberry pi doesn't have a high speed interrupt input for scanning high speed input and analog to digital converter (ADC) for scanning analog input, therefore, an additional controller is needed for sensor interface. Therefore, an Arduino Nano is used for interfacing sensors. Arduino Nano has two interrupt that can be used for high speed input scanning. It also has analog input pins for analog sensors. Arduino interfaced with raspberry pi using i2c communication.

3.5.2 Communication System

The communication is required for receiving commands and settings for robot operation. Also in future, the communication system would be used for interaction with

parent rover or satellite or other robots in the swarm group. Some of the communication protocol that were considered are Bluetooth, Wi-Fi and ZigBee. Table 4 contains the comparison between Bluetooth, Wi-Fi and ZigBee. ZigBee is low power and easy to configure. It also allows for a mesh structure which allows for long range communication by passing data in mesh. Figure 36 shows the ZigBee modem with a Sparkfun ZigBee Breakout Board. It is connected to the serial port on raspberry pi as shown in figure 45.

	ZigBee	Wi-Fi	Bluetooth
Power Requirement	Low	High	Medium
Networking Topology	Mesh	Point to hub	Ad-Hoc, very small network
Range	10 - 100 m	50 – 100 m	10 m
Number of device for network	64k	32	7

Table 4 - Comparison Between ZigBee, Wi-Fi and Bluetooth

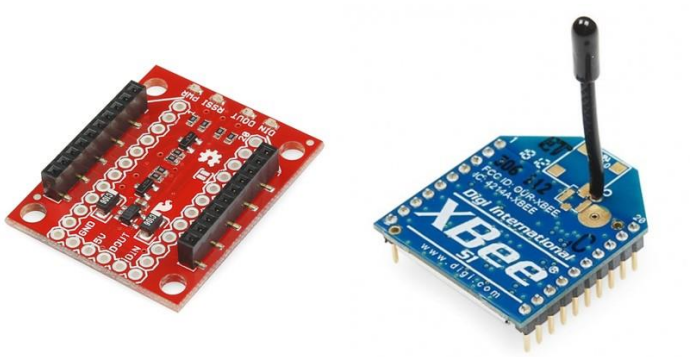

Figure 45 – ZigBee Module with Breakout Board

3.5.3 Sensors

3.5.3.1 Camera

Camera is one of the primary sensor on board. There are two cameras in the robot

Figure 47- Raspberry Pi Camera

mounted at inter-ocular distance to capture stereo images. Camera in future would be

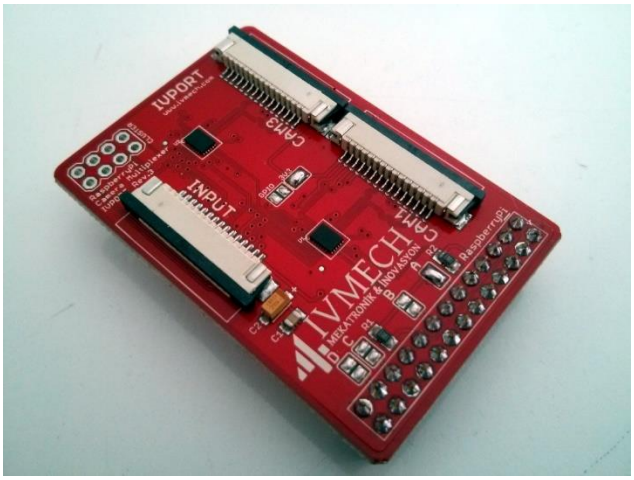

Figure 46 - Raspberry Pi Multiplexer Board

used as a navigation tool and star tracker.

Raspberry Pi board has custom built 5 MP camera board which can be connected on Camera Serial Interface (CSI) port. Raspberry Pi A+ supports only one camera. Therefore, a solution was needed to connect multiple cameras for stereo imaging. A multiplexer board from iVMech was used for the robot. The board multiplexes the CSI port on the Raspberry Pi and using I/O (Input/Output) switching can be done between cameras. Up to four cameras can be connected to the board. Stereo images is taken by sequential switching the cameras. The switching time between channels is approximately 50 ns and increase with I/O delay.

3.5.3.2 Encoders

Encoder are used as a feedback sensor for total displacement and speed of robot. Encoder can be either be incremental or absolute. We used incremental encoder

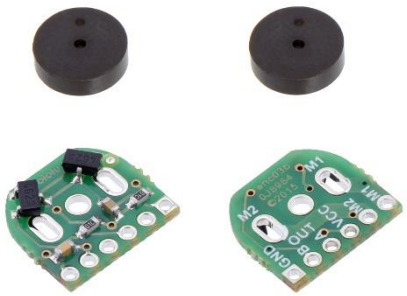

Figure 48 - Encoder for Micro Gear Motor

with two Hall Effect sensor and 6-pole magnetic disk. The encoder provides 12 counts per revolution of the motor.

3.5.3.3 Current Sensor

Current sensor is utilized to measure the power consumption of the robot. We used an ACS712 module for the robot. It measure upto 5A current. The sensor generates

Figure 49 - ACS712 Current Sensor

an analog signal and is connected to the Arduino.

3.5.4 Power System

The robot is powered by eight 3.6 V, 650 mAh lithium ion batteries. Pair of batteries are connected in series and then all the pairs in parallel. Therefore, the total

Figure 50 - Li-Ion Battery

battery output is 7.2 V, 2600 mAh. Figure 50 shows a single cell used in the robot.

A step down DC- DC voltage regulator was used to power Raspberry Pi, Arduino and sensors with 5V. SainSmart LM2596 Voltage regulator as shown in figure 51 was

Figure 52 - DC-DC Voltage Regulator

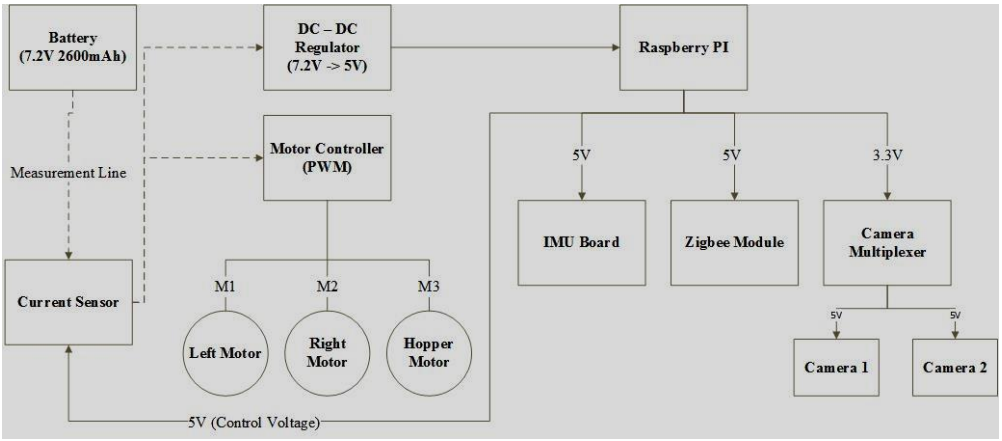

Figure 51- Power Distribution Diagram of Robot

chosen. Figure 52 shows the power distribution in the robot.

3.6 Control Software

The robot control software is divided into multiple tasks which are performed for operation of robot.

3.6.1 Command handling and data acquisition

The task runs on the raspberry pi. This task scans the serial port of Raspberry Pi

Encoder_Val_Left	Encoder_Val_Right	Current_Val	Set_Spee(	Time_Stamp
0	0	2.829515733	25	14:05.0
0	0	2.925153893	25	14:08.0
0	0	2.971916198	25	14:11.0
0	0	2.953158437	25	14:14.0
0	0	2.959763282	25	24:58.7
0	0	2.961612639	25	25:01.7
0	0	2.952365856	25	25:04.7
0	0	2.940477134	25	25:07.7
0	0	2.960820058	25	25:10.7
0	0	2.950516499	25	25:13.7
0	0	2.938891971	25	25:16.7
0	0	2.952894243	25	25:19.7

Figure 53 - Output File from Data Logger

in every cycle for commands from the laptop. If a command is received, the appropriate task perform else the task continues to perform data logging. Data are logged every 100 entries. Each entry is recorded every 30 seconds. The data logger create a new file at the start of new experiment and stores it on the local drive of raspberry pi during the experiment. This task also handles communication with the Arduino over i2c. Figure 53 shows a standard file generated by data logger.

3.6.2 Image acquisition

This task receives commands from the data handling for operation of cameras. As mentioned before, stereo images are collected by switching between cameras. Switching

is controlled by three output pin. The task sequentially switches between camera and stores the image. After every image, there is a delay of 7 ms. This is the minimum time required for storing an image on the SD card.

3.6.3 Hopping control

This task scans an input generated by the limit switch mounted such that input is received when the hopper arm reaches maximum energy point. The task stops hopping once positive edge of the signal is received.

3.7 Experimental Setup

3.7.1 Low gravity Offset and Motion Assistance and Simulation System (LOMASS)

To test the performance of the robot in low gravity condition a testbed was needed to be designed. The testbed to be designed should be able to provide multiple terrains for

Figure 54 - Design of LOMASS System

robot testing. It should be able to offset the mass of robot to simulate low gravity condition. The system should be able to move the offset mass in relation to robot position so that robot ability for motion in low gravity could be tested.

Figure 56 - Carriage with Pulleys and Suspension Cable

LOMASS was designed to meet the requirement of the experiment. Figure 54 shows the CAD model of the system. It has two parts: a sandbox for terrain and overhead

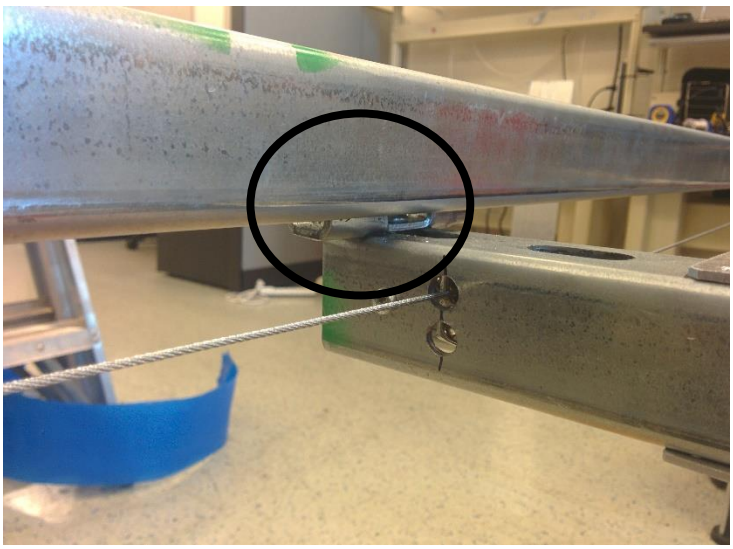

Figure 55 - Strut Channel Mounted on Trolley

motor controlled gantry. Sand box is divided into two section. Therefore, two different terrains can be setup for experiments. Partition wall is removable, thus, providing a larger area for navigation testing and path tracking for robot. Sandbox is 2m x 1m in size and has 0.2m high side walls. It is constructed out of wood.

The gantry is made of steel strut channels. The center channel is mounted on a trolleys which are housed inside the side strut channel as show in figure 56. The trolley helps in the channel to slide across the width of the sandbox. A carriage is connected to the center channel and it moves along the length of the sandbox on a trolley. Figure 55 shows the carriage with the pulleys used for suspending the robot.

As shown in the figure 57, high tension cables run across the gantry from top left corner to bottom right corner and top right corner to bottom left corner. These cables pass through the center channel helps in preventing twisting of the center channel while moving. There are two nema 23 stepper motors are used to control the X-Y motion of the carriage. The stepper motors are connected to carriage using belt drive. X axis is along the width of the gantry and Y axis is along the length of the gantry. The stepper are controlled using an Arduino and two stepper drivers. Table 4 contains specification for the LOMASS.

Maximum Travel distance X – axis	0.75 m
Maximum Travel Distance Y – axis	1.80 m
Maximum traverse speed X –axis	10 m/min
Maximum traverse speed Y-axis	20 m/min
Dimensions	2.4 m x 1.2 m x 0.6 m

Table 5 - Specification of LOMASS

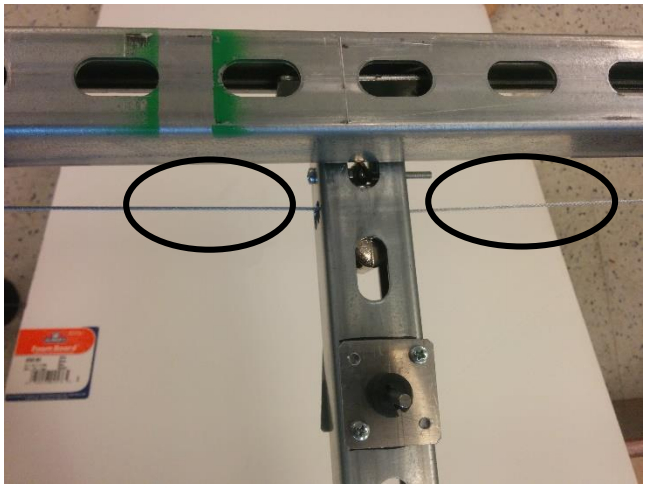

Figure 57 - Tension Cables for Preventing Twisting

3.7.2 Experimental Robot

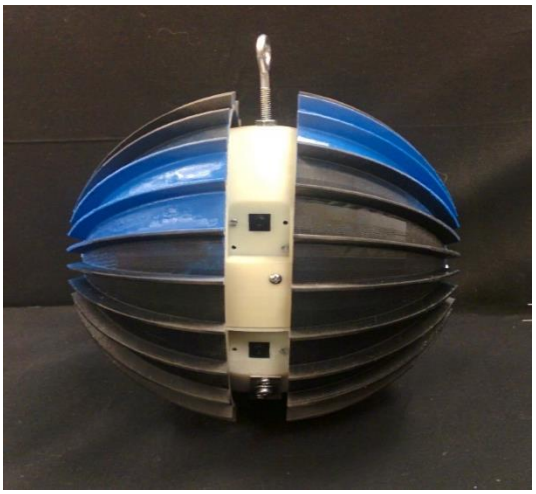

Figure 58 - Robot for Experiments

For experiment a 3D printed robot made. The robot contained all the components as per design. Robot had a hook connected to the center of the core for suspending the robot on LOMASS. The two set of wheel were printed with 7 mm and 10 mm grouser

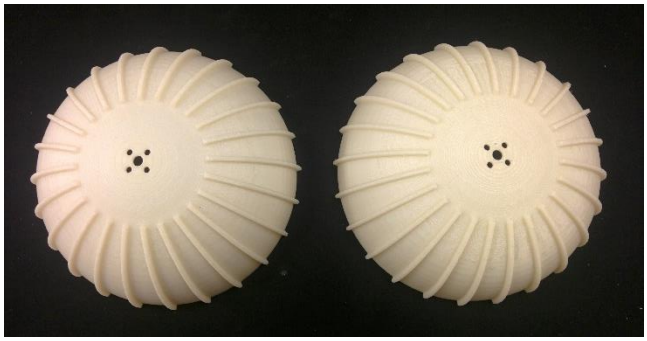

Figure 59 - Wheel with 7 mm Grouser

height as shown in figure 59 and 60 respectively. The robot was tested for mobility on different surfaces – Small rock gravels and sand. To estimate the performance in lunar and Martian condition, LOMASS was used to set the gravity offset. Robots were tested on slopes of 10° for mobility and measure the power consumption for climbing. Power consumption was measured using current sensor for steering and mobility on these surfaces. Each run was of 140 cm and the time required to travel the distance was measured.

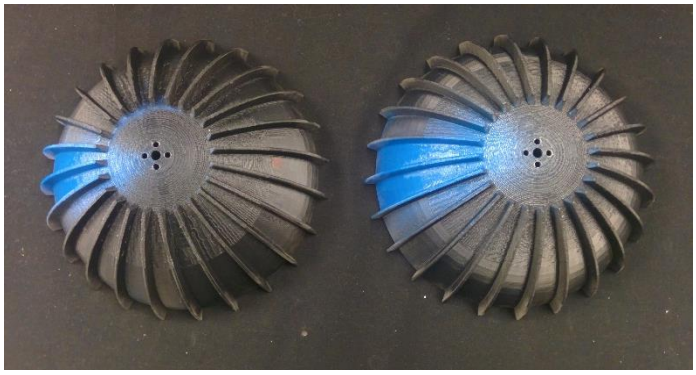

Figure 60 - Wheel with 10 mm Grouser

Hopping was tested on hard surface and height and distance of hop was measured. The robot's mass was offset to measure the performance of hopping in Lunar and Martian condition.

CHAPTER 4

RESULTS AND DISCUSSION

The robot was tested on different terrain to evaluate power and mobility. The test were performed without any guidance form the sensors and data for current and displacement was acquired. This chapter presents the acquired data and evaluates it for power required and approximate slip on different surfaces and slope for wheel with different grouser height. The chapter also present data for hopping height and power required.

4.1 Robot Performance in Lunar Gravity

4.1.1 With 10 mm High and 15˚separation Grouser Wheels

4.1.1.1 Leveled sand surface

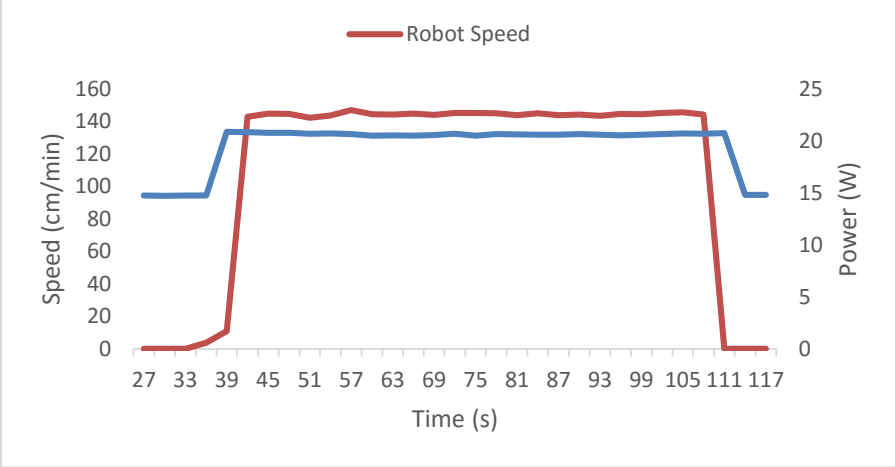

Figure 61 - Plot of Robot Speed and Power Vs Time for Levelled Sand Surface , 10 mm Grouser Height and Lunar Gravity

As discussed in previous chapter robot was tested on levelled sand surface with wheels grouser height of 10 mm. Figure 61 plots the power and robot speed based on the time. Figure 61 shows that robot requires approximately 20 W for mobility and approximately 15 W at standstill. The robot speed is also almost constant and less than set speed of 146 cm/min. Robot was observed to be travelling in approximately straight line path. Figure 62 presents a scattered plot of speed vs power during the experiment.

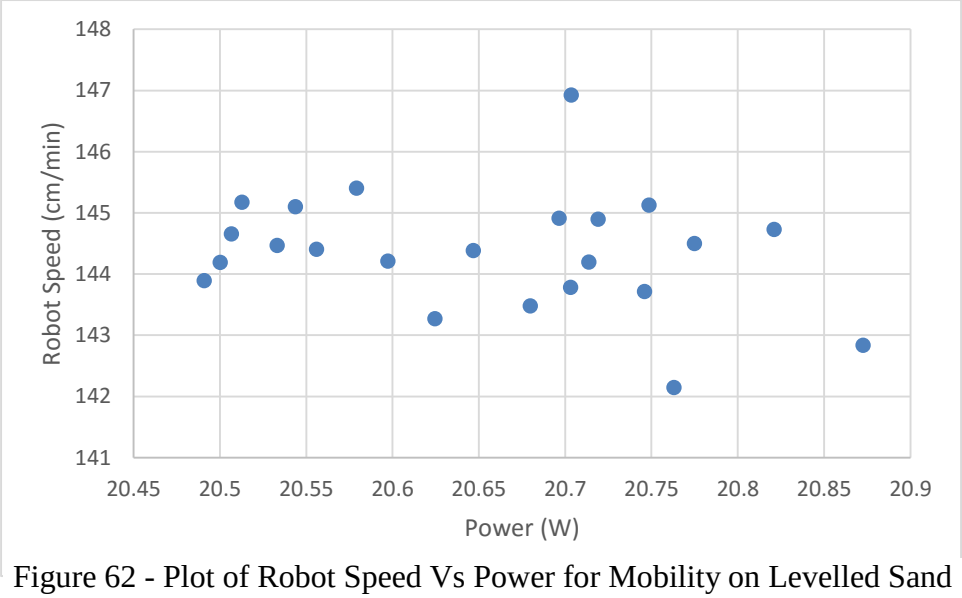

Figure 62 - Plot of Robot Speed Vs Power for Mobility on Levelled Sand Surface, 10 mm Grouser Height and Lunar Gravity

In figure 62, there are few points in the right half which represents low speed and higher power. This may be caused due to variation in the surface leveling and presence of small

slope which the robot needs to overcome whereas higher velocity would be due to downhill slopes.

As discussed in previous chapter, time was measured for the robot to travel a distance of 140 cm. The robot took 75 seconds to travel the distance. The average speed of robot was found to be 112 cm/min. The average output speed of robot was 144.36 cm/min. Therefore, the approximate slip for experiment was 22.46%. Actual slip would be lower than 22.46% due to error timing and robot not travelling in strictly straight line path. The average power for the experiment was 20.36 W

Multiple runs were done for the same setting. Table 6 tabulates the data for each run. The table shows very constant power requirement over multiple runs. Whereas the slip factor varies but variation might be due to error in path or timing. Considering errors the slip ratio is constant over multiple experiments.

Run	Average Power(W)	Time for Traverse (s)	Average slip
1	20.36	75	22.46%
2	20.84	73	21.59%
3	20.49	73	21.42%
4	20.38	76	24.86%

Table 6 - Data for Multiple Runs on Levelled Sand Surface,10 mm Grouser Height and Lunar Gravity

4.1.1.2 10˚Slope Sand Surface

As discussed in previous chapter robot was tested for mobility on slope of gradually rising slope of 10˚. The total length of run was 50 cm with 40 cm inclined plane

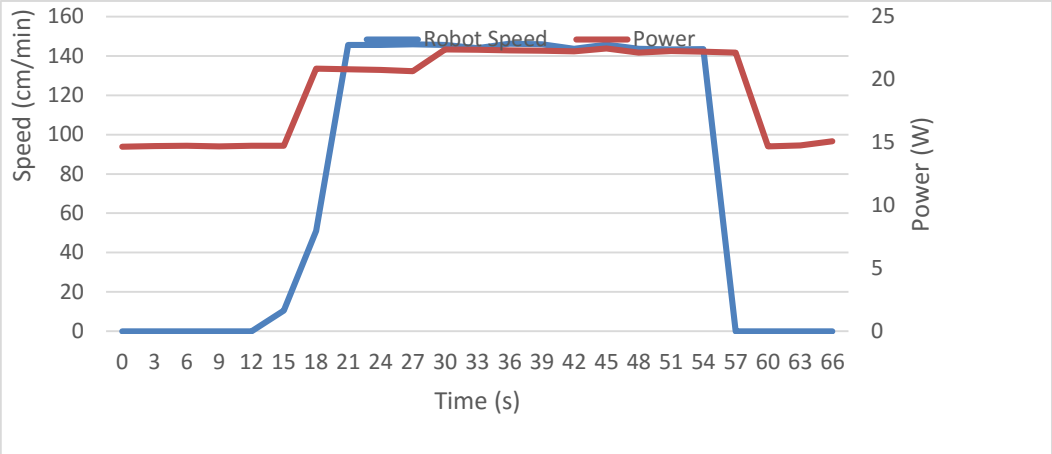

Figure 63 - Plot of Robot Speed and Power Consumption Vs Time for 10˚Slope on Sand Surface, 10 mm Grouser Height and Lunar Gravity

and 10 cm levelled surface. Figure 63 shows the variation of robot speed and power consumption with respect to time. Figure 64 shows the scattered plot of robot speed with respect to power consumption.

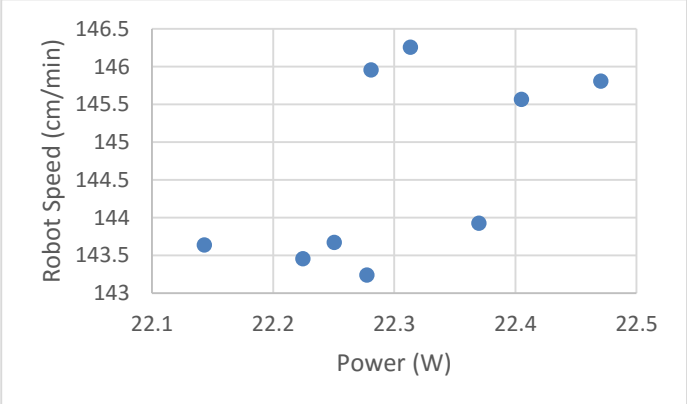

Figure 64 - Plot of Robot Speed Vs Power for 10˚Slope on Sand Surface, 10 mm Height Grouser and Lunar Gravity

Figure 63 suggest that the robot wheels speed was constant for the traverse but the power consumption increased with increase of slope. The time for traverse over slope was 31 seconds and therefore, the average speed on slope was 77.42 cm/min. Thus, the approximate slip over slope was approximately 47.26 %. From figure 64, it was observed that there are points with higher speed and lower power. Due to slip lower these point are observed in the experiment. The average power for the climbing a slope from figure 43 was 22.25 W and the average power at standstill was 14.76 W.

Run No.	Average Power (W)	Time for Traverse (s)	Average Slip
1	22.25	31	47.26%
2	23.02	30	45.48%
3	22.88	31	47.26%
4	23.06	33	50.44%

Table 7 - Data for Multiple Runs on 10˚Slope on Sand Surface, 10 mm Grouser Height and Lunar Gravity

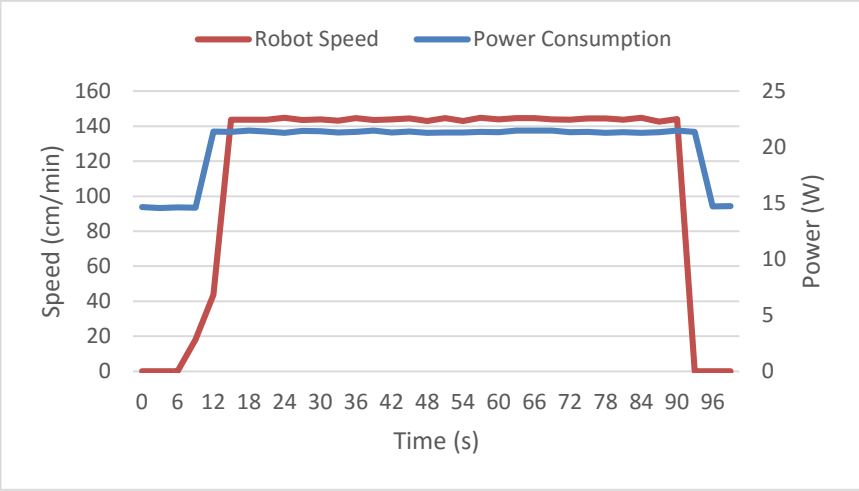

Figure 65 - Robot Speed and Power Consumption Vs Time for Small Rocky and Gravel Surface, 10 mm Grouser Height and Lunar Gravity

Table 7 suggest that average slip is constant over for multiple runs and thus actual value should be close to this value. Also the average power is consistent over multiple experiment.

4.1.1.3 Small Rocks and Gravels

As discussed in previous chapter, the robot was tested on small rock and gravels surface. The time for travelling 140 cm over the surface was measured. Figure 65 presents the plot for robot speed and power consumption over time. Figure 66 presents plot of robot speed vs the power. The time for travel was 80 sec and thus, average speed

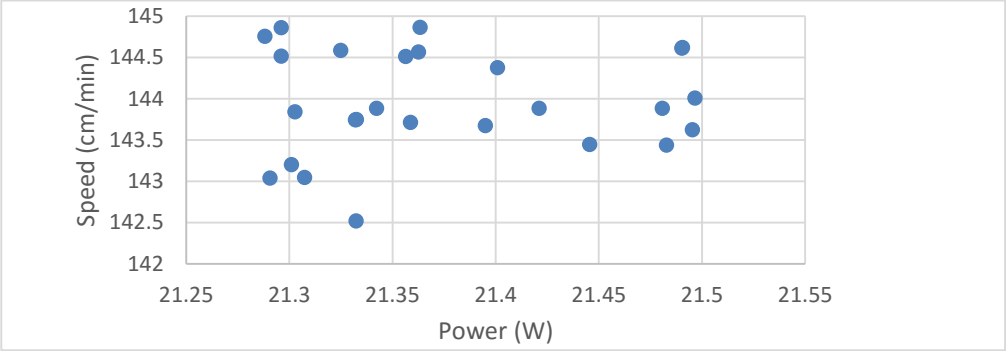

Figure 66 - Plot of Robot Speed Vs Power for Small Rocky and Gravel Surface, 10 mm Grouser Height and Lunar Gravity

for robot was 105 cm/min. Therefore, slip was approximately 28.49%. From the figure 45, the average power was 21.38 W.

The experiment shows that the robot is capable of overcoming small rocks which the robot may encounter on lunar surface. Table 8 tabulates results for multiple run on this surface. The average power shows variation due to uneven surface and thus, require varying power for traction. This also evident from the variation in slip percentage over multiple runs.

Run No	Average Power (W)	Time for Traverse (s)	Average Slip
1	21.38	80	28.49
2	22.27	82	30.19
3	20.45	80	28.49
4	21.09	84	31.85

Table 8 - Data for Multiple Run on Small Rocky and Gravel Surface,10 mm Grouser Height and Lunar Gravity

4.1.2 With 7 mm High and 9˚Separation Grouser Wheels

As discussed in previous chapter experiments were done with 7 mm high grouser wheels. The test was done on levelled sand surface. Figure 67 shows the plot of measured

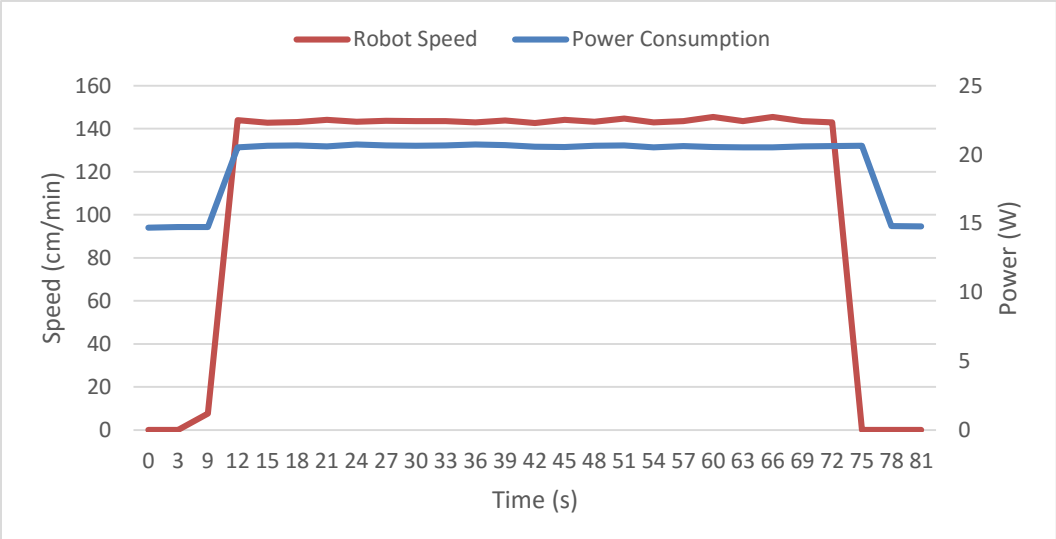

Figure 67 - Plot of Robot Speed and Power Consumption Vs Time for Levelled Sand Surface, 7 mm Grouser Height and Lunar Gravity

robot speed by encoders and power consumption over the time of run.

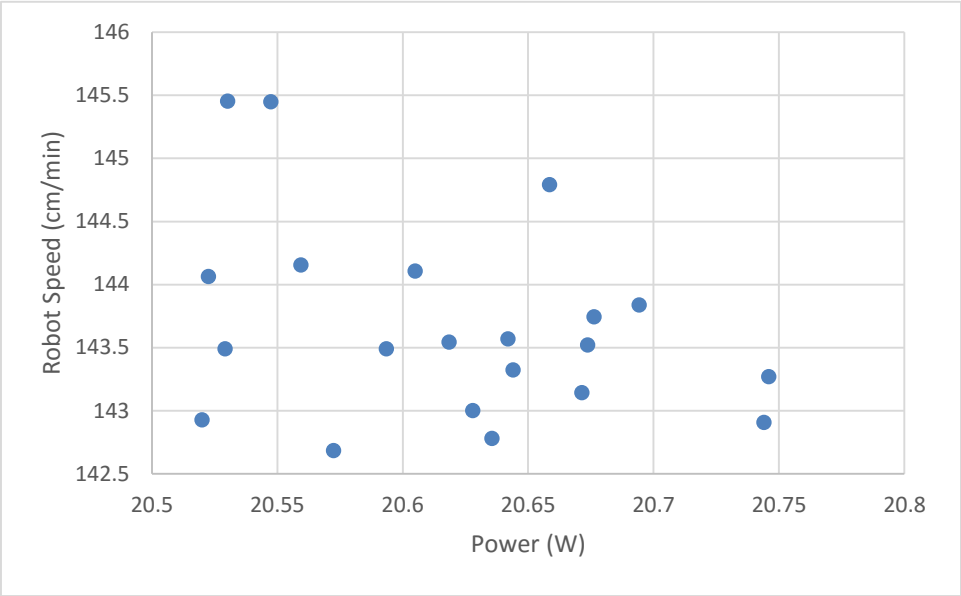

Figure 68 - Plot of Robot Speed Vs Power Consumption for Levelled Sand Surface, 7 mm Grouser Height and Lunar Gravity

Figure 68 shows that robot power consumption is not affected by the change in grouser size but there is drop in the average power during the run for this grouser size. The total traverse time for 140 cm was 68 seconds and thus, the average speed was 123.53 cm/sec which is higher as compared to wheel with 10 mm grouser height. The average slip for the run was approximately 15% which is substantially low as compared to 10 mm high grouser wheels. The average power for the run was 20.61 W

4.2 Robot Performance at Martian Gravity

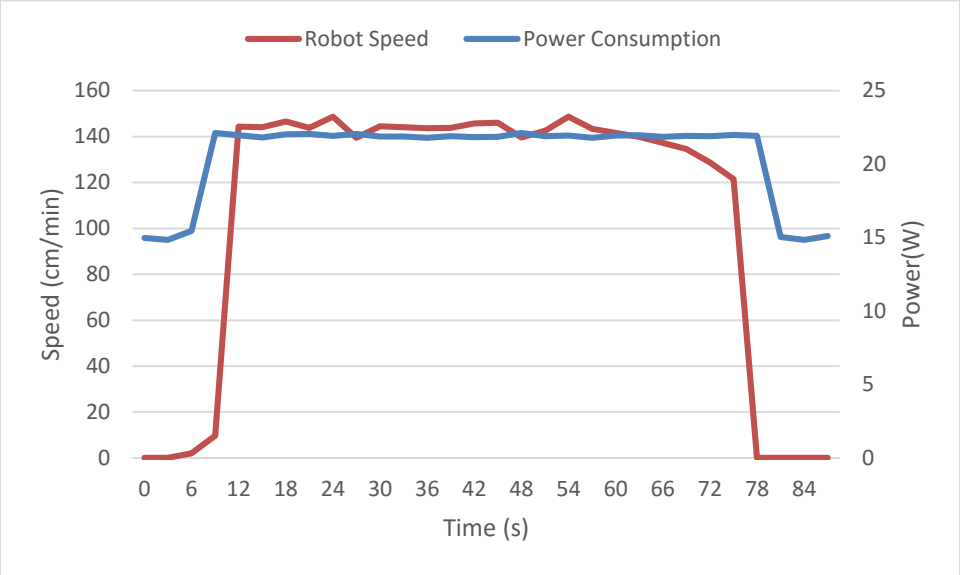

Figure 69 - Plot of Robot Speed and Power Consumption on Levelled Sand Surface, 10mm Grouser Height and Martian Gravity

The robot performance was tested in Martian Gravity on levelled sand surface with 10 mm high grouser wheels. Figure 69 shows the robot speed and power consumption over time and figure 70 show the variation robot speed with respect to power consumption during the run.

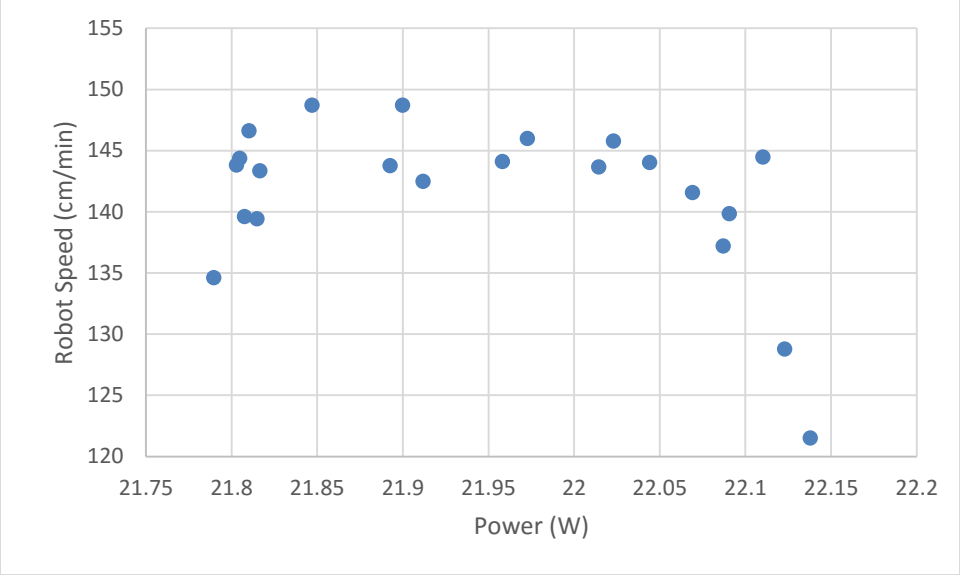

Figure 70 - Plot of Robot Speed Vs Power Consumption for Levelled Sand Surface, 10 mm Grouser Height and Martian Gravity

Figure 69 shows a decline in the robot speed at the end. This is due to lower power available for the robot from battery to drive the motor. This is not evident from the figure 61 as current sensor measures the overall power of the system and not for motors alone.

The total time for traverse of 140 cm was 62 seconds and therefore, the average speed for run was 133.33 cm/min. Thus, the average slip for the run was approximately 7%. The lower slip percentage is due to higher gravity and thus, higher traction available on mars. The average power for the run was 21.94 W which is slightly higher than power consumption on lunar surface.

4.3 Performance of Hopping Mechanism

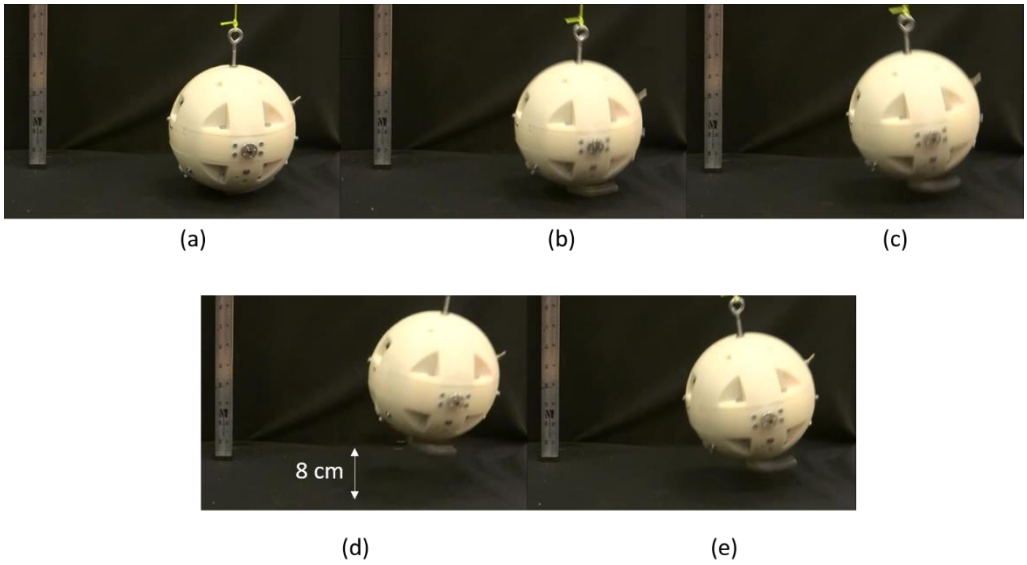

Figure 71 - Test for Operation of Hopping Mechanism at Simulated Martian Gravity

The hopping mechanism was tested for performance at simulated Martian gravity. Figure 71 shows multiple stages of hopping during test. It was observed that the robot produced a hop of 8 – 16 cm at simulated Martian gravity. The average power for each hop was around 16.40 W and time for single hop cycle was 3 seconds.

Based on above result we can extrapolate that robot will produce a hop of 16-20 cm for lunar condition. The robot performance was lower as compared to theoretically calculated hop height of 50 cm. This was due to cracking of robot plastic body during the experiment. The performance is expected to increase with metal body.

CHAPTER 5

CONCLUSION

15.1 Conclusion

- New designed for micro rover for low gravity exploration was proposed. Spherical shaped robot with two external hemispherical wheel was designed. The robot performance was found satisfactory in the controlled Laboratory environment.
- Slip percentage reduces with increase in gravity but there is increase of power consumption.
- With appropriate grouser height and grouser separation angle there is increase in average speed of the rover and the power requirement is same
- A compact hopping mechanism was designed which produces a hop of 8 - 10 cm at simulated Martian gravity. Extrapolating this, we would achieve a hop of 16- 20 cm in Lunar condition. It was calculated that robot can produce 208 hop in single charge and the robot will last 35 minutes with continuous hopping

5.2 Future Work

The future work of Ball robots will mainly focus on:

1. Developing a flight ready model of the ball robots
2. Developing techniques for obstacle avoidance and navigation. Also extend the work to development of techniques for use of ball robots for surface mapping
3. Develop algorithm for coordination between multiple ball robots to enhance capability of exploration.
4. Modify hopping mechanism for variable hop length and height.

REFERENCES

[1] Robinson,M.S., J.W.Ashley, A.K.Boyd, R.V.Wagner,E.J.Speyerer,B.Ray Hawke, H.Hiesinger, C.H.van der Bogert. "Confirmation of Sublunarean Void and Thin Layering in Mare Deposit" Planetary and Space Science Vol 69, pg 18-27, 2012.

[2] "Lunokhod: Reflections on a Moon Robot **",** Digital Image: http://apod.nasa.gov/apod/ap100606.html, Web

[3]Schilling K., Jungius C. "Mobile Robots for Planetary Exploration", Control Eng Practice, Vol 4 No.4 pg 513-524, 1996

[4]Zakrajsek, J.J., Mcissock, D.B., Woytach, J.M., Zakrajsek J.F., Oswald, F.B. , McEntire, K.J., Hill, G.M., Abel, P., Eichenberg, D.J. , Goodnight T.W.,"Exploration Rover Concepts and Development Challenges", Web, 2005

[5]Miller, D.P., "Multiple Behavior Controlled Micro Robots for planetary surface mission" ,Web ,1990

[6] Michand, F., Lafontaiane, J.D., Caron, S." A Spherical Robot for Planetary Surface Exploration", Web, 2001

[7] Battern, C., Wentzlaff, D.,"Kickbot : A Spherical Autonomus Robot", Web, 2001

[8] Bruhn F.C., Kratz H., Warell J., Lagerkvist C., Kaznov V., Jones J. A., Stenmark L., "A preliminary design for a spherical inflatable microrover for planetary exploration", Acta Astronautica 63, Pg 618-631, 2008

[9] Poczontek S. A., et al.: NCSU Space Senior Design Final Report, 2009

[10] Kesner S. B., Plante J-S., Boston P. J., Fabian T., Dubowsky S., "Mobility and Power Feasibility of a Microbot Team System for Extraterrestrial Cave Exploration", IEEE International Conference on Robotics and Automation, 2007

[11] Scarfogliero U., Stefanini C., Dario P., "A Bioinspired Concept for High Efficiency Locomotion in Micro Robots: the Jumping Robot Grillo", IEEE International Conference on Robotics and Automation, 2006

[12] Kovaˇc M., Fuchs M., Guignard A., Zufferey J-C., Floreano D.," A miniature 7g jumping robot",IEEE International Conference on Robotics and Automation, 2008

[13] Hale E., Schara N., Burdick J., Fiorini P.,"A Minimally Actuated Hopping Rover for Exploration of Celestial Bodies", Web, 2000

[14] Ackerman E., "Boston dynamics sand flea robot demonstrates astonishing jumping skills", IEEE Spectrum Robotics Blog, 2012

[15] Yoshimitsu T., Kubota T., Nakatani I. Adachi T., Saito H.,"Micro-hopping robot for asteroid exploration", Acta Astronautica 52, Pg. 441 – 446, 2003

[16]Skonieczny K., Moreland S.J., Wettergreen D.S.,"A Grouser Spacing Equation for Determining Appropriate Geometry of Planetary Rover Wheels", IEEE/RSJ International conference on Intelligent Robots and Systems, 2012

[17] Sutoh M., Nagaoka K., Nagatani K., Yoshida K., "Design of wheels with grousers for planetary rovers traveling over loose soil", Journal of Terramechanics 50, Pg. 345-353, 2013

[18] Rybus T., Nicolau-Kuklinski J., Seweryn K., Barcinski T., Ciesielska M., Grassmann K., Grygorczuk J., Kraczewski M., Kowalski M., Krzewski M.,Kucinski T., Lisowski J., Przybyla R., Skup K., Szewczyk T., Wawrzaszek R., "New Planar Air-Bearing Microgravity Simulator for Verification of Space Robotics Numerical Simulation and Control Algorithms", 7th ESA 12th Symposium on Advanced Space Technologies in Robotics and Automation (ASTRA), 2013

[19] Choset H. and Kortenkamp D., "Path Planning and Control for Free-Flying Inspection Robot in Space", Journal of Aerospace Engineering, Pg 74-81, 1999

[20] Akin D., and Howard R.,. "Neutral buoyancy simulation of space telerobotics operations.", International Society for Optics and Photonics, 1992.

[21] Brown, H., and Dolan J, "A novel gravity compensation system for space robots." ASCE, 1994.

[22] Danabalan. T.L and Sahu. Shree. Niwas, "Development of gravity compensation system for satellite reflector by helium ballon," Journal of Spacecraft Technology, Vol.17, Issue.1, p. 14-19, January 2007.

[23] Xu Y., Brown B., Aoki S., Kanade T., " Mobility and manipulation of a light weight space robot", Robotics and autonomous systems , Pg 1-12, 1994:.

[24] Sato, Y., Ejiri, A., Iida, Y., Kanda, S., Maruyama, T., Uchiyama, T., and Fujii, H., "Micro-G emulation system using constant-tension suspension for a space manipulator". IEEE International Conference on Robotics and Automation, 1991.

[25] Kemurdjian, A., and U. A. Khakhanov. "Development of simulation means for a gravity forces." Robotics, ASCE, 2000.

[26] "Active Response Gravity Offload System", Digital Image: http://www.nasa.gov/centers/johnson/engineering/integrated_environments/active_response_gravity/

[27] Akima T., Tarao S., Uchiyama M., “Hybrid Micro Gravity Simulator Consisting of a High Speed Parallel Robot”, IEEE International Conference in Robotics and Automation, 1999.

APPENDIX A

DATA COLLECTED BY ROBOT FOR EXPERIMENTS

A.1 Levelled Sand Surface, 10 mm Grouser Height and Lunar Gravity

Encoder_Left	Encoder_Right	Current_Val (A)	Set_Motor_Speed (RPM)	Time_Stamp (s)
0	0	2.947081979	25	27
0	0	2.94021294	25	30
0	0	2.947874561	25	33
0	0	2.94919553	25	36
-405	-387	4.174526433	25	39
-1608	-1404	4.164222874	25	42
-16456	-15747	4.15497609	25	45
-31267	-30514	4.152598346	25	48
-46209	-45102	4.135954136	25	51
-60972	-59388	4.140709625	25	54
-75891	-73791	4.129349291	25	57
-90687	-89022	4.100023777	25	60
-105614	-103602	4.101344747	25	63
-120592	-118091	4.098174421	25	66
-135409	-132837	4.108742173	25	69
-150095	-147557	4.11939085	25	72
-164886	-162419	4.13128023	25	75
-179733	-177231	4.12825038	25	78
-194638	-191941	4.14249825	25	81
-209342	-206621	4.13531347	25	84
-224227	-221348	4.14441505	25	87
-238952	-235993	4.11308345	25	90
-253756	-250658	4.09650695	25	93
-268402	-265291	4.12021005	25	96
-283066	-280151	4.12882778	25	99
-297970	-294758	4.10499662	25	102
-312775	-309621	4.13484035	25	105
-327580	-324531	4.09953879	25	108
-342253	-339330	4.10897976	25	111
-342253	-339330	2.960820058	25	114
-342253	-339330	2.958706507	25	117

Table 9 – Data Collected by Robot on Levelled Sand Surface, 10 mm Grouser Height and Lunar Gravity

A.2 10˚Slope Sand surface, 10 mm Grouser Height and Lunar Gravity

Encoder_Val_Left	Encoder_Val_Right	Current_Val (A)	Set_Speed (RPM)	Time_Stamp (s)
0	0	2.933872289	25	0
0	0	2.943383266	25	3
0	0	2.947081979	25	6
0	0	2.94021294	25	9
0	0	2.947874561	25	12
0	0	2.94919553	25	15
-1085	-1077	4.174526433	25	18
-6304	-6294	4.164222874	25	21
-21176	-21175	4.15497609	25	24
-36065	-36032	4.19341534	25	27
-51008	-50924	4.47817679	25	30
-65888	-65793	4.47888993	25	33
-80588	-80507	4.44758789	25	36
-95553	-95432	4.42774846	25	39
-110410	-110404	4.45880656	25	42
-125088	-125088	4.44420642	25	45
-139989	-139986	4.45110912	25	48
-154589	-154741	4.46573867	25	51
-169289	-169315	4.4509822	25	54
-183951	-183971	4.4828406	25	57
-183951	-183971	2.937835196	25	60
-183951	-183971	2.9547436	25	63
-183951	-183971	3.02145634	25	66

Table 10 - Data Collected by Robot on 10˚Slope on Sand Surface, 10 mm Grouser Height and Lunar Gravity

A.3 Small Rocky and Gravel Surface, 10 mm Grouser Height and Lunar Gravity

Encoder_Val_Left	Encoder_Val_Right	Current_Val (A)	Set_Motor_Speed (RPM)	Time_Stamp(s)
0	0	2.95487227	25	3
0	0	2.9008634	25	6
0	0	2.95470009	25	9
-1863	-1851	4.27913198	25	12
-6354	-6303	4.29349022	25	15
-21028	-20999	4.2564642	25	18
-35697	-35682	4.29244655	25	21
-50409	-50332	4.29430702	25	24
-65201	-65123	4.28928657	25	27
-79860	-79779	4.29244895	25	30
-94567	-94477	4.29351371	25	33
-109175	-109134	4.27375201	25	36
-123982	-123871	4.28964019	25	39
-138599	-138568	4.26991653	25	42
-153397	-153166	4.26335502	25	45
-168105	-167963	4.27699471	25	48
-182699	-182601	4.26135414	25	51
-197490	-197358	4.29474475	25	54
-212127	-211955	4.26167816	25	57
-226935	-226752	4.29775471	25	60
-241642	-241450	4.29493182	25	63
-256410	-256237	4.28603818	25	66
-271157	-271044	4.29890817	25	69
-285865	-285741	4.29211635	25	72
-300572	-300411	4.26697567	25	75
-315380	-315136	4.28594099	25	78
-330117	-329933	4.27047498	25	81
-344795	-344631	4.28009579	25	84
-359602	-359428	4.26249112	25	87
-374183	-373973	4.27596092	25	90
-388901	-388685	4.29460843	25	93
-388901	-388685	2.92154348	25	96

Table 11 - Data Collected by Robot on Small Rocky and Gravel Surface, 10 mm Grouser Height and Lunar Gravity

A.4 Levelled Sand Surface, 7 mm Grouser Height and Lunar Gravity

Encoder_Val_Left	Encoder_Val_Right	Current_Val (A)	Set_Motor_Speed (RPM)	Time_Stamp(s)
0	0	2.94021294	25	0
0	0	2.947874561	25	3
0	0	2.94919553	25	6
-778	-777	4.141544	25	9
-15428	-15569	4.12787053	25	12
-29980	-30197	4.14976997	25	15
-44667	-44764	4.13741221	25	18
-59329	-59553	4.11255115	25	21
-74012	-74150	4.10099903	25	24
-88787	-88752	4.10863256	25	27
-103426	-103454	4.12614132	25	30
-118105	-118106	4.10483032	25	33
-132704	-132713	4.13202706	25	36
-147403	-147410	4.12777827	25	39
-162012	-161961	4.1128145	25	42
-176721	-176713	4.09528368	25	45
-191360	-191365	4.10619904	25	48
-206099	-206217	4.10922972	25	51
-220736	-220790	4.10184273	25	54
-235406	-235456	4.13259222	25	57
-250275	-250312	4.109074	25	60
-264944	-264968	4.10063063	25	63
-279814	-279824	4.10051986	25	66
-294483	-294480	4.1414319	25	69
-309052	-309136	4.13673545	25	72
-309052	-309136	2.960820058	25	75
-309052	-309136	2.958706507	25	78

Table 12 - Data Collected by Robot on Levelled Sand Surface, 7mm Grouser Height and Lunar Gravity

A.5 Levelled Sand Surface, 10 mm Grouser Height and Martian Gravity

Encoder_Val_Left	Encoder_Val_Right	Current_Val (A)	Set_Speed (RPM)	Time Interval (s)
0	0	2.993245087	25	0
0	0	2.967177533	25	3
0	0	3.091233854	25	6
-211	-203	4.42471243	25	9
-1208	-1184	4.35021309	25	12
-16003	-15894	4.39379722	25	15
-30732	-30614	4.3873669	25	18
-46209	-45102	4.38105144	25	21
-60734	-59958	4.37146918	25	24
-75591	-75492	4.39348108	25	27
-90554	-89022	4.41483006	25	30
-105501	-103602	4.36173832	25	33
-120445	-118091	4.39708683	25	36
-135260	-132637	4.40882508	25	39
-150091	-147195	4.37432528	25	42
-165003	-162076	4.36081313	25	45
-179914	-177002	4.39654502	25	48
-193803	-191646	4.40231842	25	51
-208511	-206056	4.38832485	25	54
-223224	-221732	4.41762	25	57
-237610	-236639	4.35488546	25	60
-251991	-251187	4.38942151	25	63
-266138	-265621	4.36509379	25	66
-279988	-279808	4.3990014	25	69
-293722	-293585	4.39300471	25	72
-306519	-307108	4.38918579	25	75
-318994	-319467	4.35353225	25	78
-318994	-319467	2.95153107	25	81
-318994	-319467	3.06619835	25	84
-318994	-319467	3.00658315	25	87

Table 13 - Data Collected by Robot for Traverse on Levelled Sand Surface, 10 mm Grouser Height and Mars Gravity

APPENDIX B

MASS PROPERTIES AND POWER BUDGET

B.1 Mass Budget for Robot

Subsystem	Unit	Mass (grams)	Maximum Expected Deviation	Maximum Mass
Structure	System Chassis	213	1.4	298.2
Command & Data Handling	Raspberry Pi Board	24	1.1	26.4
	Arduino	10	1.1	11
Communications	Zigbee Module + Breakout Board	9	1.1	9.9
Primary Mobility System	Motors with mount	80	1.3	104
	Motor Control Board	24	1.1	26.4
	Wheels	270	1.3	351
Second Mobility System	Hopping Mechanism	413	1.3	536.9
	Springs	10	1.2	12
Sensors	Cameras	8	1.1	8.8
	Camera Multiplexer Board	14	1.1	15.4
Power System	Batteries	136	1.2	163.2
	Power Regulator Board	40	1.1	44
			Total Mass	1600.0
			Mass Deviation	18 %
			Mass Limit	2000
			Mass Margin	20 %

Table 14 - Mass Budget of Robot for Design

B.2 Power Budget for Robot

Unit	Instrument Duty Cycle	Power (W)	Error Margin	Power Calculated (W)	Alloted Power (W)	Margin	Total Energy Required
Raspberry Pi Board+Motor Board+Camera Multiplexer Board	1	5.50	1.30	7.15	8.50	18.88	7.15
Motor	1	9.62	1.20	11.54	13.50	16.94	11.54
Camera	1	1.60	1.30	2.08	2.50	20.19	2.08
ZigBee	1	0.13	1.40	0.18	0.22	19.05	0.18
Hopping	0.2	4.32	1.30	5.61	6.50	15.74	1.12
Total Energy Consumed Per Hour				22.08			
Total Energy Available from Battery				19.24			
Maximum Operation Time (min)				52			

Table 15- Power Budget for Robot

B.3 Mass properties and Center of masss

Following center of mass and mass properties are calculate using Solidworks model.

Mass = 1190.00 grams

Volume = 772154.99 cubic millimeters

Surface area = 557029.92 square millimeters

Center of mass: (millimeters)

X = -0.81

Y = -18.64

Z = 0.13

Moments of inertia: (grams * square millimeters)

Taken at the center of mass and aligned with the output coordinate system.

Lxx = 2881843.87	Lxy = 14615.13	Lxz = 39718.15
Lyx = 14615.13	Lyy = 3027130.09	Lyz = 61164.33
Lzx = 39718.15	Lzy = 61164.33	Lzz = 3240696.12